Different frequencies and triggers of canyon filling and flushing events in Nazaré Canyon, offshore Portugal

Joshua R. Allin[1,2], James E. Hunt[1], Peter J. Talling[1], Michael A. Clare[1], Ed Pope[1,2], Douglas G. Masson[1]

[1]National Oceanography Centre Southampton, European Way, Southampton, SO14 3ZH, UK

[2]University of Southampton, Waterfront Campus, European Way, SO14 3ZH, UK

Corresponding author: J. R. Allin (jra1g13@soton.ac.uk)

Abstract

Submarine canyons are one of the most important pathways for sediment transport into ocean basins. For this reason, understanding canyon architecture and sedimentary processes has importance for sediment budgets, carbon cycling, and geohazard assessment. Despite increasing knowledge of turbidity current triggers, the down-canyon variability in turbidity current frequency within most canyon systems is not well constrained. New AMS radiocarbon chronologies from canyon sediment cores illustrate significant variability in turbidity current frequency within Nazaré Canyon through time. Generalised linear models and Cox proportional hazards models indicate a strong influence of global sea level on the frequency of turbidity currents within the canyon. Radiocarbon chronologies from basin sediment cores indicate that larger, canyon-flushing turbidity currents reaching the Iberian Abyssal Plain have a significantly longer average recurrence interval than turbidity currents that fill the canyon. The recurrence intervals of these larger turbidity currents also appear to be unaffected by long-term changes in global sea level. This indicates that the factors triggering, and thus controlling, the frequency of canyon-flushing and canyon-filling events are very different. Canyon-filling appears to be predominantly controlled by sediment instability during sea level lowstand and by storm and nepheloid transport during the present day highstand. Canyon-flushing exhibits time-independent behaviour. This indicates that a temporally random process, or summation of non-random processes that cannot be discerned from a random signal, are triggering canyon flushing events.

1 Introduction

Understanding variability in turbidity current frequency and magnitude is important for several reasons. First, turbidity currents are one of the most voluminous sediment transport mechanisms, and they create some of the largest sediment accumulations on our planet (Ingersoll et al., 2003). Second, understanding the frequency and scale of large turbidity currents informs risk assessment for undersea installations that are at risk of damage by turbidity currents, such as oil and gas infrastructure, pipelines, and telecommunications cables (Bruschi et al., 2006; Carter et al., 2012; Carter et al., 2014).

Submarine canyon systems are recessed topographic features on continental margin slopes that act as conduits for sediment transport into the deep sea (Stow et al., 1985; Normark and Piper, 1991; van Weering et al., 2002). Turbidity currents are one of the main transport processes within submarine canyon systems, and can be triggered by a wide variety of mechanisms. Potential triggers include storm activity, tidal resuspension, sediment failures (triggered in some cases by earthquakes), and river discharges (Marshall, 1978; Masson et al., 2006; Piper and Normark, 2009; Masson et al., 2011a; Talling et al., 2012; Talling, 2014).

Turbidity currents in submarine canyons are proposed to be one of two broad end-member types: filling and flushing (Parker, 1982; Piper and Savoye, 1993; Canals et al., 2006; Piper and Normark, 2009; Talling et al., 2012). Canyon-filling turbidity currents are hypothesised to slowly deposit sediment within canyons over hundreds or even thousands of years (Paull et al., 2005; Canals et al., 2006; Arzola et al., 2008; Puig, et al., 2014). Canyon-filling turbidity currents are considered to be the result of localised sediment failures, hyperpycnal flows, or storm resuspension (Marshall, 1978; Arzola *et* al., 2008; Khripounoff et al., 2009; Masson et al., 2011a; Talling et al., 2013; Talling, 2014). Canyon-flushing turbidity currents are erosive flows that remobilise and transport large volumes of this canyon-filling sediment out onto canyon-mouth fans or distal basin floors (Parker, 1982; Piper and Savoye, 1993; Xu et al., 2004; Paull et al., 2005; Piper and Normark, 2009; Kriphounoff et al.,

2012; Talling et al., 2012; Puig et al., 2014). Canyon-flushing turbidity currents have yet to be directly monitored, and are suggested to operate on much longer timescales than those that fill the canyon (Piper and Savoye, 1993; de Stigter et al., 2007; Arzola et al., 2008; Talling et al., 2013). The causes of canyon-flushing events are not clear, although they likely result from large sediment failures (Normark and Piper, 1991; Masson et al., 2006; Goldfinger et al., 2007; Piper and Normark, 2009; Hunt et al., 2013a; Talling, 2014).

1.1 Observations of canyon-filling

Previous work on the Nazaré Canyon has focussed on the factors controlling sedimentation within the upper and middle reaches of the canyon (van Weering et al., 2002; de Stitger et al., 2007; Oliveira et al., 2007; Arzola et al., 2008; Martin et al. 2011). As many as four turbidity currents have been observed in the upper canyon per year (de Stigter et al., 2007; Martin et al., 2011; Masson et al., 2011a). These frequent turbidity currents are typically the result of winter storms that re-suspend canyon sediments, but may also be the result of small intra-canyon failures (de Stigter et al., 2007; Martin et al., 2011; Masson et al., 2011a). Direct monitoring from below 4,000 m water depth indicates that turbidity currents annually reach the lower canyon. However, these flows are generally dilute, restricted to the incised thalweg, and are not considered to be erosive (de Stigter et al., 2007).

Canyon terraces at 3500 m water depth and 40 m elevation above the thalweg) record multiple thicker (>25cm) turbidites deposited over the last 1,000 years. Turbidites recorded on terraces are interpreted as the result of large flushing events by Arzola et al. (2008) and Masson et al. (2011a). Given the presence of erosive scours within the lower reaches of the canyon, it is possible that these frequent turbidity currents are erosive and flush sediment onto the canyon-mouth fan (Arzola et al., 2008). To date, no deep water (>5000 m) core descriptions have been published from Nazaré Canyon, and so our understanding of the recurrence rates of both canyon-filling and canyon-flushing turbidity currents is limited to the upper and middle canyon, above 4,000 m water depth.

1.2 Aims of the study

Recent statistical analyses of long-term (>0.15 Ma) records indicates that large volume turbidites in distal basin plains can have a temporally random distribution, and are not strongly influenced by non-random glacio-eustatic sea level variability (Hunt et al., 2013a; Clare et al., 2014). Other studies suggest that sea level is a dominant control; however, they do not consider a sufficient number of events for statistical analysis (Maslin et al., 2004; Owen et al., 2007; Lee, 2009; Smith et al., 2013). It has also been proposed that climate-driven sea level change can affect the frequency of canyon-filling turbidity currents by influencing slope stability (Vail et al., 1977; Shanmugam and Moiola, 1982; Lebreiro et al., 1997; Piper and Normark, 2001; Lebreiro et al., 2009; Brothers et al., 2013). Therefore, we first aim to determine whether the frequency of canyon-filling shows a significant correlation with glacio-eustatic sea level change.

This present study is novel because few papers provide a complete overview of the frequency of turbidity currents from the upper to lower reaches of submarine canyons and out into deep water basins. No studies to date have statistically assessed both a basin and canyon record from a single system to test for any overarching control on the recurrences of canyon-filling and canyon-flushing. Therefore, also aim to assess whether or not canyon-flushing events have similar recurrence intervals to canyon filling events, and whether their recurrence intervals have similar statistical distributions. This will help determine whether they are likely to have similar (or different) triggers (Urlaub et al., 2013; Clare et al., 2014; 2015).

2 Regional setting

The study area is located on the Western Iberian Margin between 36^{o} and 43^{o} N (Fig. 1). The shelf and continental slope is incised by several large submarine canyons, including the Setúbal-Lisbon, Cascais, Sao Vincente and Nazaré canyons. These canyons feed into 3 deep sedimentary basins; the Iberian, Tagus and Horseshoe Abyssal Plains (Fig. 1).

2.1 Nazaré Canyon

Nazaré Canyon occurs in the central-west Iberian margin, and extends from ~1 km offshore from the coastline and into the Iberian Abyssal Plain (Fig. 1). The canyon incision into the continental shelf and slope coincides with the presence of the Nazaré Fault, which runs ENE-WSW and extends across the margin. The Nazaré Canyon system is not directly fed by major rivers, as is the case with the Setúbal and Cascais Canyons to the south. Instead, Nazaré Canyon is fed largely by littoral drift sediment from smaller river systems to the north, and nepheloid transport of material to deeper sections of the canyon (van Weering et al., 2002; Oliveira et al., 2007; de Stigter et al., 2007).

The canyon itself can be divided into three sections; the upper section that extends from the canyon head to 2,000 m water depth; the middle section that spans between 2,000 and 4,000 m; and the lower section that lies below 4,000 m (Figs. 2 and 3) (Vanney and Mougenot, 1990; van Weering et al., 2002). The upper and middle sections have a steep v-shaped profile and are incised deeply into the continental shelf (200 - 2,500 m water depth), with a channel thalweg that is <100 m wide. Below 4,000 m water depth the canyon broadens to a width of 8 – 10 km and is markedly less incised into the substrate. Below 4,500 m water depth the canyon is less incised, and large levee structures have developed to the north and south of the canyon axis. These levees are between 100 and 200 m in height and taper distally into the Iberian Abyssal Plain, where they terminate at 5,300 m water depth (Arzola et al., 2008; Lastras et al., 2009).

2.2 Iberian Abyssal Plain

The Iberian Abyssal Plain is located 200 km off the western coast of Portugal between 40^{o} N and 43^{o} N and extends approximately 700 km to the northwest. The basin plain has an average water depth of ~5,300 m but can be as deep as 5,400 m. The basin is bounded by the Galicia Bank to the northeast, the Estremadura Spur to the south, and by a series of seamounts along its western margin. The total

area of the basin covers approximately 107,000 km^2. Previous work from ODP leg 149 has detailed the long-term basin infill record extending back to the Lower Cretaceous (140 Ma) (Milkert et al., 1996a; 1996b). This work demonstrated an onset of, terrestrial-derived turbidite deposition in the Iberian Abyssal Plain between 2.2 and 2.6 Ma, which continued into the late Pleistocene. Despite the extensive record from ODP drilling legs in the Iberian Abyssal Plain, very little of the recent (<100 ka) sedimentary architecture has been evaluated in detail. As a result, little is currently known about the frequency of large volume turbidity currents in the basin through the late Pleistocene.

3 Materials and methods

3.1 Piston coring

The cores used in this study have been collected by two different scientific campaigns. Piston cores JC27-51, JC27-47 and JC27-46 come from the abyssal plain and levee sections, and were recovered during cruise JC027. Core JC27-51 was retrieved from the Iberian Abyssal Plain, and cores JC27-46 and JC27-47 were retrieved from the northern external and internal levees respectively (Fig. 3). The piston cores from the middle section of Nazaré Canyon were retrieved during cruise CD157. Cores were sited using bathymetric and geophysical data. Cores D15738 and D15739 were both collected from terraces 40 - 60 m above the canyon axis and have existing radiocarbon dates (Figs. 2 and 3). There are no sediment cores from the upper canyon above 2,000 m water depth from which AMS radiocarbon ages could be determined. The coarse-grained nature of the sediment in the upper canyon, the rapid rate of accumulation, and the tidally-driven re-working of material prevent any long-term record of turbidity currents being obtained through piston or gravity coring techniques (de Stigter et al., 2007).

3.2 Identification of turbidites and hemipelagite

In order to develop age models and determine recurrence intervals for turbidity currents, differentiating their deposits from background hemipelagic sediment is vital. Hemipelagic sediments typically contain randomly dispersed foraminifera giving a pitted surface texture. They also lack primary sedimentary structures and are often bioturbated (Stow and Piper, 1984). In contrast, turbidity current deposits are often well sorted, have normal grading, and have observable internal structure. The fine-grained mud cap of turbidity currents is commonly homogenous and often devoid of foraminiferal material, while the basal contact of turbidites is often sharp and sometimes erosional (Bouma, 1962: Stow and Piper, 1984).

Cores were logged for sedimentary features such as grain size, sedimentary structures and colour. The cores were logged using a Geotek^{TM} multi-sensor core logger (MSCL) for petrophysical data, particularly optical lightness and spectral reflectance. ITRAX-XRF geochemical data were obtained for JC27-51 to aid in the construction of the age-model using hemipelagic sediment. It has been shown that hemipelagic sediment in basin settings has a chemistry that is distinct from terrestrially-derived siliciclastic sediment, primarily due to a high proportion of detrital carbonate (Croudace et al., 2006). Where ITRAX-XRF data were not available, optical lightness (L*) was used to discriminate between Turbidite and hemipelagic deposits. High amounts of foraminiferal carbonate in basin sediments result in a lighter colour than terrestrially derived mass-flow deposits (Balsam et al., 1999).

3.3 Age model development

Age control for this study is provided by AMS radiocarbon dating. AMS radiocarbon dates were obtained for cores JC27-51, JC27-47 and JC27-46 in order to develop age models and calculate turbidity current recurrence intervals. Nine AMS radiocarbon dates were previously determined for terrace cores D15738 and D15739 (Masson et al., 2010) (Table 1). Samples were taken from hemipelagic mud units, with care being taken to avoid sampling any turbidite mud or coarse turbidite bases. In cores JC27-51, JC27-47 and JC27-46, 2 - 10 cm^3 of sediment was sampled to pick the 8 - 10 mg of foraminifera required for accurate AMS 14C dates. No one foraminiferal species was abundant

enough to collect monospecific samples in all cases, so most samples consist of mixed species assemblages. The dominant species were *Orbulina universa, Globigerina bulloides, Neogloboquadrina pachyderma, Globorotalia truncatulinoides, Globigerinoides ruber* and *Globorotalia hirsute*. Where monospecific samples were possible, *Orbulina universa* was selected. The conventional radiocarbon ages returned from analysis were converted to calibrated ages (Cal years BP) using the MARINE13 database (Reimer et al., 2013) (Table 1).

In order to account for local reservoir offsets, an average of five reservoir correction (ΔR) values was used from nearby locations. These ΔR values are from samples collected along the Iberian shelf; the main pathway for ocean currents and sediment transport to the head of Nazaré Canyon (Monges Soares, 1993; van Weering et al., 2002; Oliveira et al., 2007; de Stigter et al., 2007). This yields a ΔR correction value of +267 years, which is consistent with reconstructed past reservoir offsets along the Iberian Margin (Bronk Ramsey et al., 2012).

Using the radiocarbon ages, and the thicknesses of hemipelagic sediment between them, sedimentation rates were calculated. The thicknesses of hemipelagic sediment were then divided by the sedimentation rates to convert them into time intervals (Wynn et al., 2002; Grácia et al., 2010; Clare et al., 2014). From these time intervals the ages of individual turbidites can be estimated (Table 2; Suppl. info.). This method relies on the assumption that there is minimal fluctuation in the rate of hemipelagic sediment accumulation through time (Lebreiro et al., 2009; Grácia *et al*, 2010; Clare et al., 2015). It also relies on the assumption that subsequent turbidity currents are not significantly erosive (Weaver and Thomson, 1993; Thomson and Weaver, 1994; Weaver, 1994; Wynn et al., 2002; Gutiérrez-Pastor et al., 2009; Grácia et al., 2010).

3.4 Calculation of turbidite recurrence intervals and frequency

Using the age model to estimate the emplacement age of each turbidite allows us to calculate individual recurrence intervals. Here we define the recurrence interval of a turbidite as the length of

time since the turbidite that preceded it (Clare et al., 2014; 2015; Pope et al., 2015). Where hemipelagic age models cannot be constructed, we calculate recurrence interval by diving the length of time by the number of turbidites to get an 'average recurrence interval'. The determination of recurrence intervals requires that individual turbidites be distinguished from multiple upward-fining units deposited during the same turbidity current. These multiples of upward-fining sediment can result from differential sorting due to changing bed-shear stresses, or from multi-staged failures. (Piper and Bowen, 1978; Stow and Shanmugam, 1980; Hunt et al., 2013b). Interpreting multiple upward-fining units within a single turbidite as multiple individual turbidites has the potential to bias any analysis by the incorrect counting of turbidites; and hence, incorrectly estimating their recurrence intervals (Lebreiro et al., 2009).

3.5 Statistical analysis of turbidite recurrence and frequency

Statistical analysis can be a powerful tool for the analysis of time series data, such as turbidite recurrence (e.g. Hunt et al., 2014; Moernaut et al., 2015; Ratzov et al., 2015); however, it is important to understand how recurrence is measured before specific tests are selected. Recurrence is here inferred from intervals of hemipelagic fallout between turbidity currents, and the average accumulation rate of hemipelagic mud between dated horizons. This method is most appropriate in distal basin settings, such as basin core JC27-51 where past work has shown there is little or no erosion by successive turbidity current, and the hemipelagic mud is not removed (Weaver and Thomson, 1993; Thomson and Weaver, 1994; Weaver, 1994; Wynn et al., 2002; Gutiérrez-Pastor et al., 2009; Grácia et al., 2010; Clare et al., 2014). In more proximal, slope and confined settings, the effects of erosion may be greater, but it is difficult to discern this from core samples due to their relatively narrow diameter (typically 10 cm). We therefore bin the data at the more proximal levee core site JC27-46, by counting the number of turbidites within prescribed time intervals to account for this uncertainty in the precise measurement of individual recurrence intervals. As bin dimensions can potentially affect the statistical outcome (Urlaub et al., 2013; Pope et al., 2015) we consider three different bin widths (250, 500 and 1000 years) in our analysis. We investigate the influence of sea

level on binned turbidite recurrence at levee site JC27-46, where sufficient turbidites were sampled (N=201) to permit regression and survival analysis. In addition to different data bin sizes, we also use three different sea level curves as our explanatory variable. The sea level reconstructions of Lambeck et al. (2014), Rohling et al. (2010), and Peltier and Fairbanks (2006) are widely used and have suitable resolution over the late Pleistocene. Less sophisticated frequency analysis is used for individual turbidite recurrence intervals at basin site JC27-51, as fewer turbidites were sampled (N=26) thus limiting the power of statistical tests (Pope et al., 2015).

3.5.1 Assessing the significance of sea level on turbidite recurrence at JC27-46

We use two different statistical analyses to investigate the significance of sea level in relation to turbidite recurrence at JC27-46. The first is a parametric Generalised Linear Model, which tests for the significance of sea level as an explanatory variable on the recurrence of turbidites (McCullagh and Nelder, 1989; Clare et al., 2016). As it is a parametric test, the Generalised Linear Model requires *a priori* definition of the distribution form of the relationship between the two variables. We apply variants of the model using Gamma, Gaussian and Poisson distribution forms, and assess the most appropriate model using quantile-quantile (Q-Q) plots. While Q-Q plots do not provide a quantitative measure of the goodness-of-fit, they can be qualitatively interpreted to understand how much a given data set deviates from the specified distribution (Salkind and Rasmussen, 2007).

General rules of thumb exist for determining the minimum sample size for regression analysis. Tabachnick and Fidell (2007) indicate that testing for the effect of one individual variable will require N=106 events. Green (1991) performed a more detailed analysis, which incorporated an assessment of statistical power and effect size, suggesting that at least N=23 is required to detect large effects and N=53 for detecting medium effects of one explanatory variable. We also apply a non-parametric Cox Proportional Hazards (PH) Model (Cox, 1972) as a comparative test because it requires no *a priori* specification of frequency distribution form. The Cox PH model is typically used to determine a hazard rate in medical studies (e.g. rate of patient fatality) but has also been applied to turbidite

frequency analysis (Hunt et al., 2014; Clare et al., 2016). The hazard rate is the ratio between the change in the explanatory variable (e.g. sea level) and the response variable – in this case turbidite recurrence. Previous work has shown that the Cox PH model requires at least a minimum sample size of N=20 (Vittinghoff and McCuloch, 2007). The Cox PH model performs survival analysis and three separate tests (likelihood, Wald and log-rank), for which a p-value is derived. For both Generalised linear and Cox PH models, where the resultant p-value is small (<0.05) sea level is found to be a significant variable to explain turbidite recurrence. Where the p-value is large (p>0.05), sea level cannot be implicated as a statistically significant control on turbidite recurrence. Levee core site JC27-46 features N=201 turbidites, which is well above the minimum sample size threshold for both regression and survival analysis. Distal basin core JC27-51 only features N=26 turbidites, which is at the minimum sample size limit, and therefore would yield only low statistical power. Therefore, we simply analyse the frequency distribution form of turbidite recurrence at JC27-51 to provide insights into triggering and possible controls, instead of performing more sophisticated survival or regression analysis.

3.5.2 What is the frequency distribution form of turbidite recurrence at JC27-51?

A Poisson distribution implies time-independence and a lack of memory in a system (Parzen, 1962). Thus, recurrence intervals that fit a Poisson (exponential) distribution form can be viewed as occurring randomly in time, with no dependence on when the previous event occurred, or when the next will happen. This memoryless, time-independent behaviour is in contrast to non-random processes such as sea level change. Therefore, where recurrence intervals conform to a Poisson distribution, non-random processes cannot be directly attributed to a singular or dominant control on recurrence (Urlaub et al., 2013; Clare et al., 2014). In contrast, time-dependent distributions may indicate that a single process (e.g. Normal) or series of processes (e.g. log-normal) are exerting significant control on a system (van Rooij et al., 2013; Clare et al., 2016). Therefore, we aim to determine the frequency distribution form of turbidite recurrence intervals at JC27-51 to provide some insights into possible triggering and controlling mechanisms for canyon flushing events. We also aim to determine whether the frequency

distribution form of turbidite recurrence at the basin plain is distinctly different to that observed at the more proximal levee location.

Here we employ parametric and non-parametric goodness-of-fit methods to test recurrence interval distribution. The Anderson-Darling test is a parametric test that tells us the probabilities that the data come from different populations with specific distributions, including Poisson, normal, log-normal and Weibull (Stephens, 1974). To further test the distribution of canyon flushing events, we use non-parametric (Mann-Whitney and Kolmogorov-Smirnov) tests to determine if the frequency distribution form of Iberian Basin turbidite recurrence is significantly different to that of other distal basin plains. For this, we use the published dataset of Clare et al. (2014; 2015), which demonstrates that multiple basin turbidite records conform to a Poisson distribution. The Mann-Whitney test is based on the null hypothesis that the datasets are sampled from populations with identical distributions (Lehmann and D'Abrera, 2006). The Kolmogorov-Smirnov test compares the cumulative distributions of two data sets and poses the null hypothesis that they were randomly sampled from populations with identical frequency distributions (Lehmann and D'Abrera, 2006). The result tells us the probability that the two cumulative frequency distributions would be as far apart as observed in our data. We use these three tests to provide confidence in our results.

4 Results

4.1 Core sedimentary characteristics

Core JC27-51 shows a depositional sequence comprised of pale grey mud units with abundant foraminifera interbedded with well sorted and normally-graded sedimentary units (Fig. 3). The graded units are often greater than 50 cm thick and many are mud-dominated (Fig. 4A). Some of these mud-dominated deposits exhibit thin silt or fine sand bases. Three deposits within the core have sandy bases, with one of these (core depth 320 - 390 cm) having a much thicker medium- to coarse-grained sand base with planar and ripple laminations (Fig. 4B). We interpret these graded units as turbidite

deposits after Bouma (1962), and Stow and Piper (1984). A silt unit with interspersed mud clasts occurs at 395 - 420 cm depth in the core, and has a subtle reverse-to-normally graded sequence (Fig. 4C), which we interpret as a debrite, in the sense of Naylor (1980).

The pale sediment in core JC27-51 exhibits different colour, grain size, and lightness characteristics than turbidite deposits (Fig. 5A). Unlike the more homogenous olive-green turbidites, the pale grey sediment is noticeably rich in foraminiferal sand and exhibits bioturbation structures. This foraminiferal sand gives the sediment a pitted surface texture. From the photospectrometer data the pale grey sediment in JC27-51 exhibits an L* value typically within a range of 50 - 65, while turbidites are typically within 35 - 50. From the ITRAX XRF Calcium counts (kcps) data, the pale grey sediment typically exhibits values greater than 160 kcps (Fig. 5A). In contrast, turbidite deposits have values ranging from 40 to 120 kcps. These differences in the geochemical and geophysical properties are likely due to the high amounts of calcareous foraminiferal shells within the sediment. We interpret this pale grey sediment as background hemipelagic accumulation, after Stow and Piper (1984) and Hoogakker et al. (2004). Typically, the boundaries between the upper turbidite mud cap and the following hemipelagic sediment are gradational (Fig. 5A). This is due largely to bioturbation, but also likely due to the slow settling of turbidite mud suspension clouds and incorporation of carbonate material from background hemipelagic sediment. The boundaries between the bases of the turbidite deposits are flat and sharp (Fig. 5A).

Core JC27-46 consists largely of interbedded silt and fine sand units that are normally graded and typically have thin mud caps (Fig 4). These graded deposits can be broadly classified into two different types. Type 1 deposits are normally graded, with 1 - 4 cm thick silt or fine sand bases, and thicker 10 - 20 cm upper mud units. Type 2 deposits are thinly-bedded and have 0.5 - 4 cm thick, faintly gradational fine- to medium-grained sand bases. The thin sand bases typically grade sharply into a thin (0.5 - 3 cm) fine-grained mud (Fig. 4D and E). Type 1 deposits are dominant in the upper 6 m of the core, while type 2 are dominant in the lower 4 m. We interpret these deposits to be the result of turbidity currents in the sense of Stow and Shanmugam (1980). Within the core there are lighter,

pale grey units that are rich in foraminiferal sand, have a pitted surface, and show evidence of bioturbation. Based on the similarity with hemipelagic deposits from core JC27-51 we also interpret these to have a hemipelagic origin.

Core JC27-47 is dominated by thicker sand-rich, normally-graded deposits with medium- to coarse-grained sand bases (Fig. 4F and G). Sand units vary between 0.5 and 20 cm thick and grade sharply into fine-grained mud. Several of these deposits have clear erosional bases, with several units presenting a chaotic texture and uneven or folded bedding (Fig. 4G). We interpret deposits with normal grading and erosional bases to be turbidites (Fig. 4F). Deposits with folded bedding or chaotic texture are interpreted to be the result of small-scale slumping or debris flows after Shanmugam et al. (1995). The upper 60 cm of the core contains of the same pale grey, bioturbated and foraminiferal-rich sediment present in cores JC27-46 and JC27-51. As with the two previous cores, we interpret this to be hemipelagic sediment. Hemipelagic sediment is not present below 60 cm depth in the core, possibly due to erosion from subsequent turbidites over-spilling the internal canyon levee (Fig. 3).

Middle canyon cores are located on terraces at 40 - 60 m elevation above the canyon thalweg (Fig. 3). Cores D15738 and D15739 are composed largely of clay with interspersed faintly-graded fine sand or silt beds (Fig. 3). These are interpreted by Arzola et al. (2008) as turbidite deposits resulting from turbidity currents that overspill onto canyon terraces. Basal contacts between the sand and the underlying mud are typically erosional, and previous work indicates there is no discernible hemipelagic material between turbidite units due to the high level of shelf-derived terrigenous material transported in nepheloid layers to deeper in the canyon (de Stigter et al., 2007; Arzola et al., 2008).

4.2 Age model and sedimentation rate

Seven AMS radiocarbon dates were collected from JC27-51, five from JC27-46 and five from JC27-47 (Fig. 3). Using these dates and the known thickness of hemipelagic sedimentation, age models place the base of core JC27-51 at ca 83,000 Cal years BP and the base of core JC27-46 at ca 33,500

Cal years BP (Fig. 6). Linear regressions on the age models yielded R^2 values of 0.9934 and 0.9975 in cores JC27-51 and JC27-46 respectively (Fig. 6). These values give us a high level of certainty in a stable hemipelagic sedimentation rate over long periods at both core sites (Swan and Sandilands, 1995). Average hemipelagic sedimentation rates for cores JC27-51 and JC27-46 are 2.3 and 7.8 cm/ka respectively (Fig. 6).

Individual turbidite ages derived from the two age models can be seen in Table 2, and in Supplementary Table 1. Due to the presence of multiple erosive sandy turbidites in core JC27-47, hemipelagic material is only discernible in the upper 60 cm (Fig. 3). Below 60 cm core depth, hemipelagic sediment is sparse and indistinguishable from fine-grained turbidite deposits. Similarly in cores D15738 and D15739, hemipelagic deposits contain a high percentage of terrigenous mud with sparse foraminifera, and are therefore indistinguishable from turbidite muds (Arzola et al., 2008; Masson et al., 2011a). AMS radiocarbon dates from cores JC27-47, D15738 and D15739 originate from foraminifera collected out of bulk sediment samples. Because of the uncertainty in correctly defining hemipelagic thicknesses, recurrence intervals for each deposit cannot be calculated using a hemipelagic age model. Instead, an average turbidity current recurrence interval is calculated by dividing the number of turbidites by the time between radiocarbon dates (Fig. 3).

4.3 Regular filling events in the middle canyon

Previously collected AMS radiocarbon ages from middle canyon terrace cores place the bases of cores D15738 and D15739 at ca 1,500 BP and ca 1,000 BP respectively. Core D15738 contains 25 identifiable sandy turbidite bases above the oldest AMS radiocarbon date, while core D15739 has 21 turbidites above the oldest radiocarbon date (Fig. 3). By dividing the time interval by the number of turbidites we are able to calculate an average recurrence for turbidites. This gives us give an average turbidity current recurrence of 43 years on terraces that are 40 - 60 m above the canyon floor.

4.4 Sea level control on canyon-filling in JC27-46

For visual comparison of sea level and turbidite frequency, we use the 500 year binned turbidite data from core JC27-46 (Fig. 7A). This 500 year interval is considered to be an appropriate resolution for the length of the record (Lebreiro et al., 2009). Turbidite frequency in core JC27-46 on the external levee crest is highly variable during the sea level lowstand from 33.5 to 23.5 ka; the 10,000 year period prior to North Atlantic warming and associated sea level rise (Clark et al., 2004; Anders and Carlson, 2012) (Fig. 7A). From the modelled ages for turbidites, an average of the estimated recurrence intervals during lowstand conditions is 68 years, lower than at any point during the 33,500 year record.

Turbidite frequency decreased to 0 – 3 events per 500 years during the period from 23 and 19.5 ka, the onset of sea level transgression (Fig. 7A). This initial decline of turbidite frequency starting at 23 ka occurred considerably before the rapid global eustatic sea level rise at 20 ka (Chappelle, 2002; Peltier and Fairbanks, 2006; Clark et al., 2009; Rohling et al., 2009; Lambeck et al., 2014). Following the onset of rapid sea level rise at 17 - 19 ka (Clark et al., 2004; 2009), there is an increase in frequency (4 turbidites/500 years) that lasts until 15.5 ka. Turbidite frequency decreased significantly after 15 ka towards the Younger Dryas. An average of recurrence intervals for the global sea level transgression is 300 years. Following the onset of the present-day sea level highstand at ~7 ka there is an average of recurrence intervals of 1625 years (Fig. 7A).

A similar pattern of increasing recurrence intervals through the period of deglaciation can be seen in JC27-47 (Fig. 7B). The recurrence interval values for turbidites are also broadly comparable to those recorded in JC27-46 on the external levee for the same time period. In JC27-47, recurrence intervals are approximately 120 years at the beginning of sea level transgression at 20 ka. During the end of the sea level transgression the average recurrence interval increases to 320 years, similar to the 300 year recurrence rate found in JC27-46 (Fig. 7A and B). As in core JC27-46, following the onset of the present-day highstand at 7 ka, recurrence intervals have increased to >1000 years (Fig. 7B).

The results of generalised linear models indicate that sea level is a significant explanatory variable ($p<0.05$; Supplementary table 2) in relation to the frequency of late Pleistocene canyon-filling turbidity currents at JC27-46. As observed visually, periods of lowered sea level correspond to more frequent turbidity currents. This correlation holds for individual and binned (250, 500 and 1000 year) recurrence intervals, against all of the sea level curves that are considered by this study (i.e. (Rohling et al., 2010; Peltier and Fairbanks, 2006; Lambeck et al., 2014; Suppl. Table 2). A Gaussian distribution appears to best parameterise the relationship. Cox Proportional Hazard Models also indicate a significant influence of sea level on the turbidite recurrence for all but two model runs; a significant relationship was not observed when the Lambeck et al. (2014) sea level curve is analysed against 250 year-bins and individual turbidite recurrence (Suppl. table 2).

4.5 Time-independent canyon-flushing in JC27-51

The most recent turbidite present in core JC27-51 from the Iberian Abyssal Plain dates to ca 4,850 Cal years BP, while the oldest dates to ca 82,000 Cal years BP (Table 2). Based on a hemipelagic sedimentation rate of 2.3 cm/ka (Fig. 6) a lack of hemipelagite between two turbidites indicates a short recurrence interval. Turbidity currents in the basin are assumed to be non-erosive, and so two or more turbidites with no intervening hemipelagite are assumed to be near-synchronous, and are assigned a recurrence interval of 0 years (Table 2). This gives a 2,880 year average of recurrence intervals for flushing turbidity currents that reach the Iberian Abyssal Plain.

We compare the recurrence intervals for JC27-51 with data from four other distal basin plains (Clare et al., 2014; 2015). When recurrence intervals are normalised to the mean value for each dataset, they all fit an approximately straight line fit on an exceedance plot (Fig. 8), which is indicative of an exponential distribution. Non-parametric Mann-Whitney and Kolmogorov-Smirnov tests demonstrate statistically that the distribution form of turbidite recurrence at JC27-51 shows no significant difference to the four other exponentially-distributed basin plain records (Supplementary Table 3). Given the relatively small sample size (i.e. N=26), it is possible that we do not have sufficient

turbidites to make a fully conclusive statement, but we can state that it is not possible to differentiate the recurrence record from other time-independent records. The Mann-Whitney and Kolmogorov-Smirnov tests also allow us to demonstrate that the frequency distribution form of turbidite recurrence in the basin plain (JC27-51) is significantly different ($p<0.0001$) to the time-dependent recurrence at levee location JC27-46. Thus, recurrence intervals for canyon-flushing turbidites in the Iberian Abyssal Plain may be considered time-independent and occurring at a significantly different tempo and to that of canyon-filling flows.

5. Discussion

In this section we first discuss the triggers and controls on canyon-filling turbidity currents in Nazaré Canyon, and how external factors such as sea level affect recurrence rates. Second, we discuss the possible triggering mechanisms for large canyon-flushing turbidity currents. Finally, we evaluate the implications of these findings for geohazard assessment and in light of future climate change predictions.

5.1 Canyon-filling in the present day highstand

The process of canyon-filling occurs on a variety of different temporal and spatial scales within Nazaré Canyon. Previous monitoring in Nazaré Canyon has documented as many as four turbidity currents may occur in the upper canyon per year (de Stigter et al., 2007; Martin et al., 2011; Masson et al., 2011a). These small and frequent turbidity currents do not appear to deposit on canyon levees, or the abyssal plain, as there is a general absence of turbidites deposited more recently than 3 ka (Figs 3, and 7A and B). These sub-annual turbidity currents are confined primarily to the incised canyon thalweg and typically dissipate before reaching depths greater than 4,000 m water depth (Fig. 9A). One turbidity current recorded by de Stigter et al. (2007) below 4,000 m water depth also did not appear to deposit on canyon levees or on the abyssal plain. These flows may erode previously emplaced sediment, but are not considered to flush large volumes of material (Fig. 9A).

Terrace cores at 3,500 m water depth and 40 m elevation above the thalweg reveal a mean recurrence of 43 years for larger turbidity currents over the last 1,000 years. These distal turbidite deposits are interpreted as the result of large flushing turbidity currents by Arzola *et al.* (2008), although there is no evidence of post 1 ka deposits in the Iberian Abyssal Plain that would indicate canyon-flushing has occurred (Fig. 4, and 7A and B). Given the presence of erosive scours within the lower reaches of the canyon, it is possible that these frequent turbidity currents are erosive and do flush sediment from for the upper to the lower canyon, but are too small to overtop levees or reach the abyssal plain (Fig. 9A) (de Stigter et al., 2002; Arzola et al., 2008). However, no age-models exist for lower canyon cores making this difficult to support.

5.2 Canyon-filling during sea level lowstand

The role of sea level lowstand in exposing continental shelves and resulting in more terrigenous sediment delivery to slope and deep-sea fans is widely accepted; as is the role of canyons as conduits for this sediment delivery (Vail et al., 1977; Shanmugam and Moiola, 1982; Posamentier et al., 1991; Piper and Savoye, 1993; Lebreiro et al., 1997; Clark and Mix, 2000; Ducassou et al., 2009; Lebreiro et al., 2009; Covault and Graham, 2010). Our hemipelagic age model reveals that the frequency of canyon-filling turbidity currents was highest during sea level lowstand (Fig. 7A and B). Lowstand-dominated canyons typically occur when the canyon does not incise the entire continental shelf (Covault and Graham, 2010). During highstand conditions such canyons are not in direct contact with the shoreline or fluvial sources, limiting sediment delivery. During sea level lowstand, sequence stratigraphic models predict direct connection between rivers and canyon heads. This results in a higher frequency of turbidity currents due to increased sediment supply and associated instability (Shanmugam and Moiola, 1982; Stow et al., 1984; Posamentier et al., 1991; Piper and Savoye, 1993; Lebreiro et al., 2009; Covault and Graham, 2010).

During sea level lowstand the larger area of exposed continental shelf likely resulted in greater erosion and littoral sediment delivery to the Nazaré Canyon head (Fig. 9B) (Posamentier et al., 1991; Sommerfield and Lee, 2004; Durán et al., 2013). Despite the lack of a direct fluvial sediment supply into Nazaré Canyon, there are a number of small river systems to the north which feed onto the continental shelf (Fig. 9B). Increased sediment supply to the shelf from these river systems during lowstand conditions may also have led to increased littoral sediment transport, and contributed to the higher frequency of turbidity currents being generated (Fig. 9B). It is also possible that these river systems were routed across the shelf and into the canyon head during sea level lowstand, although there is no geomorphic evidence available to support this.

Lebreiro et al. (2009) have suggested that slope instability in the Setúbal/Lisbon and Cascais Canyons (Fig. 1) is highest during sea level transgression. This implies that large turbidity currents that fill the Setúbal/Lisbon and Cascais Canyons switch-off at 15.5 ka. Work by Masson et al. (2011b) instead demonstrates that the Setúbal/Lisbon and Cascais Canyons experience an almost complete switch-off in large canyon-filling turbidity current activity at 6.6 ka. The switch-off of canyon-filling activity in the Setúbal/Lisbon and Cascais Canyons proposed by Lebreiro et al. (2009) at 15.5 ka could more easily be explained by the 200 m elevation of their core site. This elevation above the canyon would bias the record towards the largest turbidity currents (de Stigter et al., 2011). Our age models and statistical analyses from Nazaré Canyon also indicate that large canyon-filling turbidity currents switch-off at ~7 ka (Fig. 9B). This is suggestive of a margin-wide sea level control on large-scale canyon-filling in Portuguese Margin canyons.

5.2.1 Uncertainties of the statistical analyses

The results of the generalised linear models and Cox proportional hazards models indicate that sea level is well correlated with turbidite frequency recorded on the external canyon levee (Supplementary table 2). While sea level is generally accepted as having a dominant control on sedimentation in many other deep sea fan settings, our results should be treated with some caution. Our data set contains 201

557 turbidites, and while this is a sufficient number for regression-based analyses (Green, 1991;
558 VanVoorhis and Morgan, 2007), it is smaller than many other datasets used in statistical analyses of
559 recurrence (Clare et al., 2014; 2015). The height of the JC27-46 core site above the canyon floor may
560 also bias the turbidite record towards those turbidity currents large enough to over-spill the outer
561 levee. There may also be turbidite deposits that are not visually detectable because they are sub-
562 millimetre in scale. Moreover, the sea level curves used in this study are all global (eustatic)
563 reconstructions, and may not be suitable for local analysis where the effect of eustatic sea level
564 changes may be outweighed or convoluted by localised isostatic and tectonic influences (Shanmugam
565 and Moiola, 1982; Stow et al., 1984; Covault and Graham, 2010; Romans et al., 2015). Importantly,
566 binning the data appears to have an effect on the significance of sea level. 500 year and 1000 year bin
567 sizes appear to be less significant or not significant when tested against sea level (Supplementary
568 Table 2). This has also been observed in other statistical analyses of turbidite recurrence (Urlaub et al.,
569 2013; Pope et al., 2015)
570
571 **5.3 Potential triggers of canyon-flushing**
572
573 The frequency distribution of canyon flushing flows in Nazaré Canyon is indicative of temporally
574 random, time-independent behaviour. A temporally random distribution can result from *a)* a single
575 temporally random or pseudo-random process, *b)* numerous non-random processes affecting a single
576 source overprinting and resulting in a random distribution, *c)* several different sources feeding into the
577 same basin, or *d)* shredding of environmental (triggering) signal due to the long recurrence intervals
578 (Urlaub et al., 2013; van Rooij et al., 2013; Clare et al., 2014; 2015; Pope et al., 2015; Romans et al.,
579 2015). Here we will evaluate different processes that could trigger canyon-flushing events.
580
581 ***5.3.1 Are large storms a trigger?***
582
583 It has been stated that storms have the potential to trigger turbidity currents that transport sand into
584 deep water (TsuTsui et al., 1987; Shanmugam, 2008). Within Nazaré Canyon, storm-triggered

turbidity currents play a significant role in small-scale canyon-filling during the present day (Fig. 9A) (van Weering et al., 2002; de Stigter et al., 2007; Martin et al., 2011; Masson et al., 2011a). One of the limiting factors in assessing the role of storms in canyon-flushing events is the length of the observational record. Meteorological data available for the last 63 years indicates that there have been over 150 storms (wave height >1.6 m) recorded since 1952 (Lozano et al., 2004; Almeida et al., 2011). Despite the number of storm events, we see no recent turbidite deposits in the levee or abyssal plain cores; however, the cores may not contain the most recent sediments due to sampling loss. If storms had been a trigger of canyon-flushing through the Holocene, we would expect to see turbidites throughout Holocene sedimentary sequences. It may be possible that some extremely rare storms are large enough to generate turbidity currents that are erosive and capable of flushing the canyon. The lack of turbidites observed in the Iberian Abyssal Plain during last 2,000 years, combined with the likely number of storm events, makes it improbable that storms are a trigger of canyon-flushing (Fig. 3 and table 2).

5.3.2 Is sea level control undetectable due to 'signal shredding'?

Certain sedimentary environments serve as ideal long-term archives of climatic or environmental signals. This is particularly true in the case of deep-water fan and continental slope settings. In these deep-water settings, one of the principal expressions of sea level variability is changes in down-system sediment transport (Stow and Piper, 1984; Posamentier et al., 1991; Covault and Graham, 2010; Covault et al., 2010).

Signal shredding can be defined here as the filtration of environmental signals through a system by a non-linear process; in this case sediment transport (Jerolmack and Paola, 2010; Romans et al., 2015). Environmental signals like sea level may be considered a linear input into a system. However, the recording of this signal in sedimentary archives by sediment transport and deposition is typically non-linear. This is because sediment transport and deposition is highly variable and dependent on several initial and transport conditions. For turbidity currents these can include the triggering mechanism,

sediment volume, run-out distance, and whether or not these currents bypass or deposit (Piper and Normark, 2009; Talling et al., 2013, Talling, 2014). These preconditions impart non-linearity that can ultimately filter or 'shred' the signal of environmental change. In the case of Nazaré canyon-filling turbidity currents, the sea level signal is preserved in the levee due to the number of events recorded, the proximity to source, and the regularity with which they were deposited. The height of the levee above the canyon also likely prevents smaller, more frequent events triggered by storm or wave activity from depositing at the core site. Storm and wave activity could be considered a separate environmental signal and may mask the longer-term sea level signal (Romans et al., 2015).

In contrast to this, canyon-flushing events are typically less frequent, often having recurrence intervals of >2000 years (Fig. 9 and Table 2). They involve the remobilisation of sediment stored within the canyon over many thousands of years (Paull et al., 2005; Talling et al., 2007; Piper and Normark, 2009; Talling, 2014). This implies that if canyon-flushing events are the result of climatic variability or change, their rarity (non-linearity) in the depositional record could have shredded any signal of this climatic control (Covault and Fildani, 2014; Clare et al., 2015; Romans et al., 2015). Such signal-shredding could explain the temporally random distribution of canyon-flushing events in the Iberian Abyssal Plain.

5.3.3 Are regional earthquakes a trigger?

Turbidite paleoseismology involves the use of marine or lacustrine turbidite recurrence rates as a proxy for earthquake recurrence. This method has been applied to numerous settings to develop estimates of long-term earthquake hazard rate (Adams, 1990; Monecke et al., 2004; Goldfinger et al., 2007; Polonia et al., 2013; Moernaut et al., 2014, 2015). Sumner et al. (2013) outline four independent criteria for identifying an earthquake trigger for turbidites: 1) synchronous turbidites in multiple basins; 2) observing an identical number of turbidites above and below the confluence of submarine channels; 3) identifying a larger relative volume for turbidites compared with others deposited in the same setting; 4) a historical or observational record of an earthquake that is coeval with the turbidite.

Nazaré canyon has three branching channels, with confluences at 500 and 3,000 m water depth (Fig. 2) (Lastras et al., 2009). There are no sediment cores positioned directly below or above these confluences, making the confluence test of Adams (1990) unsuitable in this study area. Due to a lack of core coverage in the basin it is also impossible to estimate turbidite volumes and invoke a seismic trigger. Turbidite paleoseismology has been previously applied to the Iberian margin and a catalogue of Late Quaternary seismo-turbidites exists for the Tagus and Horseshoe Basins (Fig. 10A) (Garcia-Orellana et al., 2006; Gràcia et al., 2010; Masson et al., 2011b). This serves as a basis to test for earthquake triggering of turbidites in the Iberian Abyssal Plain.

Comparison with published Iberian turbidite records reveals that only three turbidites correlate well into the adjacent Tagus Abyssal Plain (TAP), and only one turbidite is well correlated in all three basins (Fig. 10A). Other large turbidites from the Iberian Abyssal Plain (IAP) are not synchronous with proposed seismo-turbidites from the Tagus or Horseshoe Abyssal Plain. The Iberian Margin contains multiple faults as a result of the compressional rotation associated with the Azores-Gibraltar fracture zone to the south (Fig. 10B) (Buforn et al., 1988; Borges et al., 2001; Zitellini et al., 2004; Custódio et al., 2015). The Nazaré Fault (NF) and the Lower Tagus Valley Fault (LTVF) are quite proximal, suggesting that large earthquakes originating from the LTVF might be capable of triggering sediment failures which ignite and flush Nazaré Canyon (Fig. 10B) (Johnston, 1996). This could explain why several turbidites are synchronous in both the Tagus and Iberian Abyssal Plains (Fig. 10A).

The tectonic regime along the south-western section of the Iberian Margin is more complicated, with several extensive offshore faults capable of generating large earthquakes (Fig. 10B) (Pro et al., 2013; Custódio et al., 2015). There is 300 km distance from the south-west margin to Nazaré Canyon, and there is no continuous fault system between the areas. Paleoseismic intensity reconstructions and seismic propagation models indicate large earthquakes along the south-western section of the margin are unlikely to trigger canyon-flushing in Nazaré Canyon (Dobrovolsky et al., 1979; Buforn et al.,

1988; Fukushima and Tanaka, 1990; Johnston, 1996; Zitellini et al., 2004). This could explain why several turbidites present in the Tagus and Horseshoe Abyssal Plain are not present in the Iberian Abyssal Plain (Fig 10A).

The synchronous deposition test does not strongly support regional earthquakes as a trigger for canyon-flushing turbidites in the Iberian Abyssal Plain. The historical record of large Portuguese earthquakes extends back to the Portugal and Galicia Earthquake at 60 BC (Galbis, 1932; Baptista and Miranda, 2009). Several earthquakes dating further back to 7,000 Cal years BP have been inferred from onshore paleo-tsunami records (Ruiz et al., 2008). Importantly, these records place the epicentres of many of these past earthquakes along the South-western Iberian Margin, and not proximal to Nazaré Canyon. This also makes them unsuitable as an independent earthquake archive with which to compare Iberian Abyssal Plain turbidite ages.

The Nazaré Fault (NF) forms part of a larger NNE-SSW-trending Variscan fault system which extends across the peninsula (Fig. 10B) (Buforn et al., 1988; Zitellini et al., 2004). Paleoseismic reconstructions on these NNE-SSW trending fault zones in Central and Northern Portugal are sparse, and no such record exists for the Nazaré Fault. This makes identifying possible earthquake triggering of canyon-flushing from nearby faults problematic. Optically Stimulated Luminescence (OSL) dates from fault surfaces along the Manteigas-Bragança Fault (MBF) north-east of the Nazaré Fault reveal three large (Mw 7.3) earthquakes between 11.5 and 14.5 ±2 ka, (Fig. 10A). These ages do not correspond well with turbidites in the Iberian Abyssal Plain, although the wide margins of error do encompass 2 turbidites at 11.7 ka and 14.9 ka (Fig. 10A). It has been proposed that these NNE-SSW-trending Variscan faults primarily accommodate reverse faulting and not strike-slip faulting. In contrast, WNW–ESE-trending faults on the South-western Iberian Margin exhibit strike-slip behaviour (Borges et al., 2001; Custódio et al., 2015). This would imply that unlike the southwestern margin, earthquakes along the Central Portuguese Margin do translate down-fault, limiting seismic propagation (Sylvester, 1988).

A small number of turbidites from the Iberian Abyssal Plain can be correlated with seismo-turbidites previously identified in the Tagus and Horseshoe Abyssal Plains (Fig. 10A). Turbidites which do not correlate in the Tagus or Horseshoe Basins could be the result of earthquakes originating from further north along the ENE-SSW Fault zone. However, given the wide uncertainties on earthquake ages, and the structure of the fault system, any correlation with canyon-flushing events would be largely speculative. There are multiple other intraplate faults that may trigger canyon-flushing, but without accurate paleoseismic records it is impossible to imply causation (Buforn et al., 1988; Zitellini et al., 2004; Villamor et al., 2012; Custódio et al., 2015). The lack of convincing evidence for earthquake triggered canyon-flushing along this margin highlights the problems of applying turbidite paleoseismology methods to structurally complex margins.

5.3 Climate change and geohazard implications

As previously outlined, many authors have suggested that large continental margin failures are associated with times of significant climatic and sea level change (Maslin et al., 2004; Owen et al., 2007; Lee, 2009; Smith et al., 2013; Brothers et al., 2013). One implication of this is that future climate and sea level change might increase the frequency of large continental margin failures. Our findings contribute to a growing body of literature that suggests large sediment failures in multiple settings are temporally random and are not significantly influenced by climate or sea change (Beattie and Dade, 1999; Urlaub et al., 2013, 2014; Clare et al., 2014; Hunt et al., 2014; Moernaut et al., 2014; Talling et al., 2014). It might be reasonable to conclude that the recurrence intervals of large sediment failures and canyon-flushing along the Central Iberian Margin will not be significantly influenced by any future sea level rise. Canyon-flushing in other deep-sea canyons is currently poorly understood and few estimates of recurrence rates exist. Additional work into other canyon systems would help to determine if temporal randomness is a wide-spread characteristic of canyon-flushing.

Our statistical analysis demonstrates that sea level is a significant control on canyon-filling. However, the current sea level highstand features limited canyon-filling events. These are typically small,

channel-confined turbidity currents that die before reaching the lower canyon (Fig 9A). Intuitively, we might expect future sea level rise to further limit canyon-filling turbidity currents, as past sea level rise did. However, future sea level rise has been predicted to increase rates of coastal erosion (Gornitz, 1991; Bray and Hooke, 1997; Leatherman et al., 2000). This increase in sediment delivery to the Iberian Shelf could lead to an increase in littoral transport into the head of Nazaré Canyon, thereby promoting greater instability. These smaller turbidity currents may not have large geohazard implications, but are important for assessing risk to seafloor structures such as pipelines and telecommunication cables.

6. Conclusions

Canyon-flushing turbidity currents have been predicted to occur much less frequently than those that fill canyons (Paull et al., 2005; Canals et al., 2006; Arzola et al., 2008; Puig, et al., 2014). Here we demonstrate that canyon-flushing turbidity currents in this system have recurrence rates of several thousands of years on average. This recurrence rate is an order of magnitude longer than those filling the canyon during sea level lowstand, and more than two orders of magnitude longer than those that fill the canyon in the present day. The recurrence intervals for canyon-filling and canyon-flushing appear to have distinctly different statistical distributions. Moreover, unlike canyon filling, the recurrence rate of canyon-flushing events does not appear to be affected by long-term changes in sea level. This suggests that they may have different triggers, or that the signal of triggering mechanisms is shredded due to the long recurrence intervals. From a geohazard assessment perspective, this implies that the frequency of potentially hazardous canyon-flushing events may not be influenced by future sea level predictions. The tectonic complexity of the margin, uncertainties in age-control, and the time-independent behaviour of canyon-flushing make determining a trigger for canyon-flushing problematic; although earthquakes may trigger some events.

Acknowledgements

753 The authors wish to thank Michele Rebesco, David Piper, and an anonymous reviewer. Their
754 comments and suggestions have greatly improved this manuscript. Financial support for this work was
755 provided by the Marine Geoscience group at the National Oceanography centre, and by the NERC
756 Arctic Research Programme (NE/K00008X/1). This research was completed as part of the EU FP7-
757 funded ASTARTE (Assessment, Strategy and Risk Reduction for Tsunamis in Europe) Project
758 (603839).

759

760 References:

761

762 Abraimov, S.G., Turcotte, D.L., Shcherbakov, R., Rundle, J.B., Yakovlev, G., Goltz, C., Newman,
763 W.I., 2008. Earthquakes: Recurrence and interoccurrence times. Pure and Applied Geophysics
764 165, 777-795.

765 Adams, J., 1990. Paleoseismicity of the Cascadia subduction zone: Evidence from turbidites off the
766 Oregon-Washington margin. Tectonics 9, 569–583.

767 Ahmad, M.I., Sinclair, C.D., Werritty, A., 1988. Log-logistic flood frequency analysis. Journal of
768 Hydrology 98, 205-224.

769 Almeida, L.P., Ferreira, Ó., Vousdoukas, M.I., Dodet, G., 2011. Historical variation and trends in
770 storminess along the Portuguese South Coast. Natural Hazards and Earth System Sciences 11,
771 2407–2417.

772 Alves, T.M., Gawthorpe, R.L., Hunt, D.W., Monteiro, J.H., 2003. Cenozoic tectono-sedimentary
773 evolution of the western Iberian margin. Marine Geology 195, 75-108.

774 Arzola, R.G., Wynn, R.B., Lastras, G., Masson, D.G., Weaver, P.P.E., 2008. Sedimentary features and
775 processes in the Nazaré and Setúbal submarine canyons, west Iberian margin. Marine
776 Geology 250, 64-88.

777 Balsam, W.L., Deaton, B.C., Damuth, J.E, 1999. Evaluating optical lightness as a proxy for carbonate
778 content in marine sediment cores. Marine Geology 161, 141-153.

779 Baptista, M.A., Miranda, J.M., 2009. Revision of the Portuguese catalogue of tsunamis. Natural
780 Hazards and Earth System Sciences 9, 25–42.

781 Beattie, P. D., & Dade, W. B. (1996). Is scaling in turbidite deposition consistent with forcing by
782 earthquakes? Journal of Sedimentary Research 66 (5), 909-915.

783 Bondevik, S., Svendsen J.I., Johnsen, G, Mangerud, J and Kaland, P.E., 1997. The Storegga tsunami
784 along the Norwegian coast: Its age and run-up. Boreas 26, 29–53.

785 Borges, J., Fitas, A.J.S., Bezzeghoud, M. & Teves-Costa, P., 2001. Seismotectonics of Portugal and its
786 adjacent Atlantic area, Tectonophysics 331 (4), 373–387.

787 Bouma, A.H., 1962. Sedimentology of some Flysch Deposits: A Graphic Approach to Facies
788 Interpretation. Elsevier, Amsterdam, pp. 168.

789 Bray, M.J., Hooke, J.M., 1997. Prediction of soft-cliff retreat with accelerating sea-level rise. Journal
790 of Coastal Research 13 (2), 453-467.

791 Bronk Ramsey, C. *et al*et al., 2012. A Complete Terrestrial Radiocarbon Record for 11.2 to 52.8 kyr
792 B.P.. Science 338, 370-374.

793 Brushci, R., Bughi, S., Spinazzè, M., Torselletti, E., Vitali, L., 2006. Impact of debris flows and
794 turbidity currents on seafloor structures. Norwegian Journal of Geology 86, 317-337.

795 Buforn, E., Udías, A., Colombás, M.A., 1988. Seismicity, source mechanisms and tectonics of the
796 Azores-Gibraltar plate boundary. Tectonophysics 152, 89-118.

797 Canals, M., Puig, P., de Madron, X.D., Heussner, S., Palanques, A., Fabres, J., 2006. Flushing
798 submarine canyons. Nature 444, 354-357.

799 Carlson, A.E., Winsor, K., 2012. Northern hemisphere ice-sheet response to climate warming. Nature
800 Geoscience 5, 607-613.

Carter, L., Gavey, R., Talling, P.J., Liu, J., 2014. Insights into Submarine Geohazards from Breaks in Subsea Telecommunication Cables. Oceanography 27 (2). 58-67.

Carter, L., Milliman, J.D., Talling, P.J., Gavey, R., Wynn, R.B., 2012. Near-synchronous and delayed initiation of long run-out submarine sediment flows from a record-breaking river flood, offshore Taiwan. Geophysical Research Letters 39 (12), doi:10.1029/2012GL051172.

Chappelle, J., 2002. Sea level changes forced ice breakouts in the Last Glacial cycle: new results from coral terraces. Quaternary Science Reviews 21, 1229-1240.

Clare, M. A., Talling, P. J., Challenor, P. G., & Hunt, J. E. (2016). Tempo and Triggering of Large Submarine Landslides: Statistical Analysis for Hazard Assessment. In Submarine Mass Movements and their Consequences. Springer International Publishing, pp. 509-517.

Clare, M A., Talling, P.J., Hunt, J.E., 2015. Are landslide-turbidite recurrence intervals random and what are the implications of a common distribution for triggers, regional controls and climate influence? Earth and Planetary Science Letters 420, 102-115.

Clare, M.A., Talling, P.J., Challenor, P., Malgesini, G., Hunt, J.E., 2014. Distal turbidites reveal a common distribution for large (>0.1 km^3) submarine landslide recurrence. Geology 42 (3), 263-266.

Clark, P.U., Dyke, A.S., Shakun, J.D., Carlson, A.E., Clark, J., Wohlfarth, B., Mitrovica, J.X., Hostetler, S.W., McCabe, A.M., 2009. The Last Glacial Maximum. Science 325, 710-714.

Clark, P.U., McCabe, A.M., Mix, A.C., Weaver, A.J., 2004. Rapid rise of sea level 19,000 years ago and its global implications. Science 304, 1141-1144.

Clark, P.U., Mix, A.C., 2000. Ice sheets by volume. Nature 406, 689–690.

Covault, J.A., & Fildani, A., 2014. Continental shelves as sediment capacitors or conveyors: source-to-sink insights from the tectonically active Oceanside shelf, southern California, USA. Geological Society of London Memoirs 41.1, 315–326.

825 Covault, J.A., Graham, S.A., 2010. Submarine fans at all sea-level stands: Tectono-morphologic and
826 climatic controls on terrigenous sediment delivery to the deep sea. Geology 38, 939-942.

827 Covault, J.A., Romans, B.W., Fildani, A., McGann, M., & Graham, S.A., 2010. Rapid climatic signal
828 propagation from source to sink in a southern California sediment-routing system. Journal of
829 the Geological Society of America 118, 247–259.

830 Cox, D.R., 1972. Regression models and life-tables. Journal of the Royal Statistical Society, Series B,
831 187-220.

832 Croudace, I.W., Rindby, A., Rothwell, G., 2006. ITRAX: description and evaluation of a multi-
833 function X-ray core scanner. In: Rothwell, R.G. (Ed.), New techniques in sediment core
834 analysis. Geological Society of London Special Publications 267, pp. 51–63.

835 Custódio, S., Dias, N.A., Carrilho, F., Góngora, E., Rio, I., Marreiros, C., Morais, I., Alves, P., Matias,
836 L., 2015. Earthquakes in western Iberia: improving the understanding of lithospheric
837 deformation in a slowly deforming region. Geophysical Journal International 203, 127-145.

838 de Stigter, H.C., Boer, W., de Jesus Mendes, P.A., César Jesus, C., Thomsen, L., van der Bergh, G.D.,
839 van Weering, T.C.E., 2007. Recent sediment transport and deposition in the Nazaré Canyon,
840 Portuguese continental margin. Marine Geology 246, 144-164.

841 de Stigter, H.C., Jesus, C.C., Boer, W., Richter, O.T., Costa, A., van Weering, T.C.E., 2011. Recent
842 sediment transport and deposition in the Lisbon-Setúbal and Cascais submarine canyons,
843 Portuguese continental margin. Deep Sea Research II 58 (23), 2321–2344.

844 Dobrovolsky, I.P., Zubkov, S.I., Miachkin, V.I., 1979. Estimation of the size of earthquake
845 preparation zones. Pure and Applied Geophysics 117 (5), 1025-1044.

846 Ducassou, E., Migeon, S., Mulder, T., Murat, A., Capotondi, L., Bernasconi, S.M., Mascle, J., 2009.
847 Evolution of the Nile deep-sea turbidite system during the Late Quaternary: influence of
848 climate change on fan sedimentation. Sedimentology 56, 2061-2090.

Durán, R., Canals, M., Lastras, G., Micallef, A., Amblas, D., Pedrosa-Pàmies, R., Sanz, J.S., 2013. Sediment dynamics and post-glacial evolution of the continental shelf around the Blanes submarine canyon head (NW Mediterranean). Progress in Oceanography 118, 28-46.

Fukushima, Y., Tanaka, T., 1990. A new attenuation relation for peak horizontal acceleration of strong earthquake ground motion in Japan. Bulletin of the Seismological Society of America 80 (4), 757-778.

Galbis, J., 1932. Cata´logo sı´smico de la zona comprendida entre los meridianos 5^{o} E y 20^{o} W de Greenwich y los paralelos 45^{o} y 25^{o} N, Tomo 1. Instituto Geográfico, Catastral y de Estadística, Madrid. 897pp.

Garcia-Orellana, J., et al., 2006. Identifying instrumental and historical earthquake records in the SW Iberian Margin using 210Pb turbidite chronology. Geophysical Research Letters 33, L24601. http://dx.doi.org/10.1029/2006GL028417.

Goldfinger, C., Morey, A.E., Nelson, C.H., Gutiérrez-Pastor, J., Johnson, J.E., Karabanov, E., Chaytor, J., Eriksson, A., 2007. Rupture lengths and temporal history of significant earthquakes on the offshore and north coast segments of the Northern San Andreas Fault based on turbidite stratigraphy. Earth and Planetary Science Letters 254, 9–27.

Gornitz, V., 1991. Global coastal hazards from future sea level rise. Palaeogeography, Palaeoclimatology, Palaeoecology (Global Planetary Change Section) 89, 379-398.

Gràcia, E., Vizciano, A., Escutia, C., Asioli, A., Rodés, Á., Pallàs, R., Garcia-Orellana, J., Lebreiro, S., Goldfinger, C., 2010. Holocene earthquake record offshore Portugal (SW Iberia): testing turbidite paleoseismology in a slow-convergence margin. Quaternary Science Reviews 29, 1156-1172.

Green, S.B., 1991. How many subjects does it take to do a regression analysis? Multivariate Behavioral Anaylsis 26 (3), 499-510.

873 Gutiérrez-Pastor, J., Nelson, C.H., Goldfinger, C., Johnson, J.E., Escutia, C., Eriksson, A., Morey,
874 A.E., and the Shipboard Scientific Party, 2009. Earthquake control of Holocene turbidite
875 frequency confirmed by hemipelagic sedimentation chronology on the Cascadia and Northern
876 California active tectonic continental margins. In: Kneller, B., McCaffrey, W., Martinsen, O.J.
877 (Eds.), External Controls on Deepwater Depositional Systems. SEPM Special Publication, v.
878 92. Society for Sedimentary Geology, Tulsa, OK, ISBN 978-1-56576-136-0, p. 179–197.

879 Hagiwara, Y., 1974. Probability of earthquake occurrence as obtained from a Weibull distribution
880 analysis of crustal strain. Tectonophysics 23, 313-318.

881 Hoogakker, B.A.A., Rothwell, R.G., Rohling, E.J., Paterne, M., Stow, D.A.V., Herrle, J.O., Clayton,
882 J., 2004. Variations in terrigenous dilution in western Mediterranean Sea pelagic sediments in
883 response to climate change during the last glacial cycle. Marine Geology 211, 21-43.

884 Hunt, J.E., Talling, P.J., Clare, M.A., Jarvis, I., Wynn, R.B., 2014. Long-term (17 Ma) turbidite record
885 of the timing and frequency of large flank collapses of the Canary Islands. Geochemistry,
886 Geophysics, Geosystems 15 (8), 3322-3345.

887 Hunt, J.E., Wynn, R.B., Talling, P.J., Masson, D.G., 2013a. Frequency and timing of landslide-
888 triggered turbidity currents within the Agadir Basin, offshore NW Africa: Are there
889 associations with climate change, sea level change and slope sedimentation rates? Marine
890 Geology 346, 274-291.

891 Hunt, J.E., Wynn, R.B., Talling, P.J., Masson, D.G., 2013b. Multistage collapse of eight western
892 Canary Island landslides in the last 1.5 Ma: Sedimentological and geochemical evidence from
893 subunits in submarine flow deposits. Geochemistry, Geophysics, Geosystems 14, 2159–2181.

894 Ingersoll, R. V., Dickinson, W. R., & Graham, S. A., 2003. Remnant-ocean submarine fans: largest
895 sedimentary systems on Earth. Special Papers - Geological Society of America, 191-208.

896 IOC, IHO, BODC,. 2003. Centenary Edition of the GEBCO Digital Atlas. British Oceanographic Data
897 Centre, Liverpool.

898 Jerolmack, D.J., Paola, C., 2010. Shredding of environmental signals by sediment transport.
899 Geophysical Research Letters 37, L19401, doi:10.1029/2010GL044638,

900 Johnston, A.C., 1996. Seismic moment assessment of earthquakes in stable continental regions-111.
901 New Madrid 181 1-1812, Charleston 1886 and Lisbon 1755. Geophysical Journal
902 International 126, 314-344.

903 Jorry, S.J., Jégou, I., Emmanuel, L., Silva Jacinto, R., Savoye, B., 2011. Turbiditic levee deposition in
904 response to climate changes: The Var Sedimentary Ridge (Ligurian Sea), Marine Geology
905 279, 148-161.

906 Khripounoff, A., Vangriesheim, A., Crassous, P., Etoubleau, J., 2009. High frequency of sediment
907 gravity flow events in the Var submarine canyon (Mediterranean Sea). Marine Geology 263,
908 1–6.

909 Lambeck, K., Rouby, H., Purcell., P., Sun, Y., Sambridge, S., 2014. Sea level and global ice volumes
910 from the Last Glacial Maximum to the Holocene. Proceedings of the National Academy of
911 Sciences 111 (43), 15296-15303.

912 Lastras, G., Arzola, R.G., Masson, D.G., Wynn, R.B., Huvenne, V.A.I., Hühnerbach, V., Canals, M.,
913 2009. Geomorphology and sedimentary features in the Central Portuguese submarine
914 canyons, Western Iberian margin. Geomorphology 103, 310-329.

915 Leatherman, S.P., Zhang, K., Douglas, B.C., 2000. Sea level rise shown to drive coastal erosion. Eos
916 Transactions of the American Geophysical Union 81, 55-57.

917 Lebreiro, S.M., McCave, I.N., Weaver, P.P.E., 1997. Late Quaternary turbidite emplacement on the
918 Horseshoe abyssal plain (Iberian margin). Journal of Sedimentary Research 67, 856–870.

919 Lebreiro, S.M., Voelker, A.H.L., Vizcaino, A., Abrantes, F.G., Alt-Epping, U., Jung, S., Thouveny,
920 N., Grácia, E., 2009. Sediment instability on the Portuguese continental margin under abrupt
921 glacial climate changes (last 60 kyr). Quaternary Science Reviews. 28, 3211–3223.

Lee, H.J., 2009. Timing of occurrence of large submarine landslides on the Atlantic ocean margin, Marine Geology 264, 56-64.

Lehmann, E.L., 2006. Nonparametrics: Statistical methods based on ranks, Springer, New York.

Lozano, I., Devoy, R.J.N., May, W., Anderson, U., 2004. Storminess and vulnerability along the Atlantic coastlines of Europe: analysis of storm records and of a greenhouse gases induced climate scenario. Marine Geology 210, 205-225.

Marshall, N.F., 1978. Large storm-induced sediment slump reopens an unknown Scripps submarine canyon tributary. In: Stanley, D.J., Kelling, G. (Eds.), Sedimentation in Submarine Canyons, Fans and Trenches. Dowden, Hutchinson and Ross Inc., Pennsylvania, pp. 73–82.

Martin, J., Palanques, A., Vitorino, J., Oliveira, A., de Stitger, H.C., 2011. Near-bottom particulate matter dynamics in the Nazaré submarine canyon under calm and stormy conditions. Deep-Sea research II 58, 2388-2400.

Maslin, M., Owen, M., Day, S., Lond, D., 2004. Linking continental slope-failures and climate change: testing the clathrate gun hypothesis. Geology 32 (1), 53-56.

Masson, D.G., Arzola, R.G., Wynn, R.B., Hunt, J.E., Weaver, P.P.E., 2011b. Seismic triggering of landslides and turbidity currents offshore Portugal. Geochemistry, Geophysics, Geosystems 12, doi:10.1029/2011GC003839.

Masson, D.G., Harbitz, C.B., Wynn, R. B., Pedersen, G. and Løvholt, F., 2006. Submarine landslides: processes, triggers and hazard prediction. Philosophical Transactions of the Royal Society 364, 2009–2039.

Masson, D.G., Huvenne, V.A.I., de Stigter, H.C., Arzola, R.G., LeBas, T.P., 2011a. Sedimentary features in the middle Nazaré Canyon. Deep-Sea Research II 58, 2369-2387.

McCullagh, P., Nelder, J.A., 1989. Generalized Linear Models, Second Edition. Chapman and Hall/CRC, London.

946 Mecklin, C., 2007. Q-Q Plot. In: Salkind, N.J., Rasmussen, K. (Eds.), Encyclopedia of Measurement
947 and Statistics. Thousand Oaks, CA: Sage Publications, Inc., pp. 803-805. doi:
948 http://dx.doi.org/10.4135/9781412952644.n367

949 Milkert, D., Alonso, B., Liu, L., Zhao, X., Comas, M., de Kaenel, E., 1996a. Sedimentary facies and
950 depositional history of the Iberia Abyssal Plain. In: Whitmarsh, R.B., Sawyer, D.S., Klaus, A.,
951 and Masson, D.G.. Proceedings of the Ocean Drilling Program, Scientific Results 149, Ch. 45,
952 685-704.

953 Milkert, D., Weaver, P.P.E., Liu, L., 1996b. Pleistocene and Pliocene turbidites from the Iberia
954 Abyssal Plain. In: Whitmarsh, R.B., Sawyer, D.S., Klaus, A., and Masson, D.G., Proceedings
955 of the Ocean Drilling Program, Scientific Results, 149, Ch. 12, 281-294.

956 Moernaut, J., Van Daele, M., Strasser, M., Clare, M.A., Heirman, K., Viel, M., Cardenas, J., Kilian,
957 R., Ladrón de Guevara, B., Pino, M., Urrutia, R., De Batist, M. (2015) Lacustrine turbidites
958 produced by surficial slope sediment remobilization: a mechanism for continuous and
959 sensitive turbidite paleoseismic records. Marine Geology. doi:10.1016/j.margeo.2015.10.009

960 Moernaut, et al (2014). Lacustrine turbidites as a tool for quantitative earthquake reconstruction: New
961 evidence for a variable rupture mode in south central Chile. Journal of Geophysical Research:
962 Solid Earth, 119 (3), 1607-1633.

963 Monecke, K., Anselmetti, F.S., Becker, A., Sturm, M., Giardini, D., 2004. Signature of historic
964 earthquakes in lake sediments in Central Switzerland. Tectonophysics 394, 21–40.

965 Monges Soares, A.M., 1993. The 14C content of marine shells: Evidence for variability in coastal
966 upwelling off Portugal during the Holocene in Isotope techniques. In: The Study of Past and
967 Current Environmental Changes in the Hydrosphere and Atmosphere (Proceedings) Vienna.
968 IAEA-SM-329/49. 471-485.

969 Naylor, M.A., 1980. Origin of inverse grading in muddy debris flow deposits--a review. Journal of
970 Sedimentary Petrology 50, 1111-6.

971 Normark, W.R., Piper, D.J.W., 1991. Initiation processes and flow evolution of turbidity currents:
972 implications for the depositional record. In: From Shoreline to Abyss, edited by R.H.
973 Osborne, Special Publications SEPM Society for Sedimentary Geology 46, 207 – 230.

974 Oliveira, A., Santos, A.I., Rodrigues, A., Vitorino, J., 2007. Sedimentary particle distribution and
975 dynamics on the Nazaré canyon system and adjacent shelf (Portugal). Marine Geology 246,
976 105-122.

977 Owen, M., Day, S., Maslin, M., 2007. Late Pleistocene submarine mass movements: occurrence and
978 causes. Quaternary Science Reviews 26, 958–978.

979 Parker, G., 1982. Conditions for the ignition of catastrophically erosive turbidity currents. Marine
980 Geology 46, 307-327.

981 Parzen, E., 1962. On estimation of a probability density function and mode. Annals of Mathematics
982 and Statistics 33 (3), 1065–1076.

983 Peltier, W., Fairbanks, R., 2006. Global glacial ice volume and Last Glacial Maximum duration from
984 an extended Barbados sea level record. Quaternary Science Reviews 25, 3322–3337.

985 Pinder III, J.E., Wiener, J.G., Smith, M.H., 1978. The Weibull distribution: a new method of
986 summarizing survivorship data. Ecology 59 (1), 175-179.

987 Piper, D.J.W., Savoye, B., 1993. Processes of late Quaternary .turbidity current flow and deposition
988 on the Var deep-sea fan, north-west Mediterranean Sea. Sedimentology 40, 557-582.

989 Piper, D.W.J, Bowen, A.J., 1978. Origin of lamination in deep sea, fine-grained sediments. Nature
990 274, 324-328.

991 Piper, D.W.J., Normark, W.R., 2001. Sandy fans—from Amazon to Hueneme and beyond: AAPG
992 Bulletin 85 (8), 1407-1438.

993 Piper, D.W.J., Normark, W.R., 2009. Processes that initiate turbidity currents and their influence on
994 turbidites: a marine geology perspective. Journal of Sedimentary Research 79, 347-362.

995 Polonia, A., Panieri, G., Gasperini, L., Gasparotto, G., Bellucci, L.G., Torelli, L., 2013a. Turbidite
996 paleoseismology in the Calabrian Arc subduction complex (Ionian Sea). Geochemistry,
997 Geophysics, Geosystems 14, 112–140.

998 Pope, E.L., Talling, P.J., Urlaub, M., Hunt, J.E., Clare, M.A., Challenor, P., 2015. Are large
999 submarine landslides temporally random or do uncertainties in available age constraints make
1000 it impossible to tell? Marine Geology 369, 19-33.

1001 Posamentier, H.W., Erskine, R.D., and Mitchum, R.M., Jr., 1991. Submarine fan deposition within a
1002 sequence stratigraphic framework. In: Weimer, P., and Link, M.H., eds., Seismic facies and
1003 sedimentary processes of submarine fans and turbidite systems. New York, Springer-Verlag,
1004 p. 127–136.

1005 Pro, C., Buforn, E., Bezzeghoud, M., Udias, A., 2013. Mechanism of 2003, 2007 and 2009
1006 earthquakes (S. Vicente Cape) and implications for the 1755 Lisbon earthquake.
1007 Tectonophysics 583, 16–27.

1008 Puig, P., Palanques, A., Martin, J., 2014. Contemporary sediment-transport processes in submarine
1009 canyons. Annual Review of Marine Science 6, 5.1-5.25.

1010 Ratzov, G., Cattaneo, A., Babonneau, N., Déverchère, J., Yelles, K., Bracene, R., & Courboulex, F.
1011 (2015). Holocene turbidites record earthquake supercycles at a slow-rate plate boundary.
1012 Geology 43 (4), 331-334.

1013 Reimer, P.J., Bard, E., Bayliss, A., Beck, J.W., Blackwell, P.G., Ramsey, C.B., Buck, C.E., Cheng, H.,
1014 Edwards, R.L., Friedrich, M., Grootes, P.M., Guilderson, T.P., Haflidison, H., Hajdas, I.,
1015 Hatté, C., Heaton, T., Hoffmann, D.L., Hogg, A., Hughen, K.A., Kaiser, K., Kromer, B.,
1016 Manning, S.W., Niu, M., Reimer, R., Richards, D.A., Scott, E.M., Southon, J.R., Staff, R.A.,
1017 Turney, C., Plicht, J., 2013. IntCal13 AND Marine13 radiocarbon age calibration curves 0–
1018 50,000 years cal BP. Radiocarbon 55, 1869-1887.

1019 Rockwell, T., Fonseca, J., Madden, C., Dawson, T., Owen, L.A., Vilanova, S. & Figueiredo, P., 2009.
1020 Palaeoseismology of the Variliça Segment of the Manteigas-Bragança Fault in northeastern
1021 Portugal, Geological Society, London, Special Publications 316 (1), 237–258.

1022 Romans, B.W., Castelltort, S., Covault, J.A., Fildani, A., Walsh, J.P., 2015. Environmental signal
1023 propagation in sedimentary systems across timescales. Earth-Science Reviews
1024 doi:10.1016/j.earscirev.2015.07.012.

1025 Ruiz, F., Abad, M., Vidal, J.R., Ca´ ceres, L.M., Gonza´ lez-Regalado, M.L., Carretero, M.I., Pozo,
1026 M., Toscano, F.G., 2008. The geological record of the oldest historical tsunamis in
1027 southwestern Spain. Rivista Italiana di Paleontologia e Stratigrafia 114 (1), 145–154.

1028 Shanmugam, G., Moiola, R.J., 1982. Eustatic control of turbidites and winnowed turbidites. Geology
1029 10, 231–235.

1030 Shanmugam, G., Bloch, R.B., Mitchell, S.M., Beamish, G.W.J., Hodgkinson, R.J., Damuth, J.E.,
1031 Straume, T., Syvertsen, S.E., Shields, K.E., 1995. Basin-Floor Fans in the North Sea:
1032 Sequence Stratigraphic Models vs. Sedimentary Facies. AAPG Bulletin 79 (4), 477-512.

1033 Smith, D.E., Harrison, S., Jordan, D.T., 2013. Sea level rise and submarine mass failure on open
1034 continental slopes. Quaternary Science Reviews 82, 93-103.

1035 Sommerfield, C.K., Lee, H.J., 2004. Across-shelf sediment transport since the Last Glacial Maximum,
1036 southern California margin. Geology 32, 345-348.

1037 Stephens, M.A., 1974. EDF statistics for goodness of fit and some comparisons. Journal of the
1038 American Statistical Association 69 (347), 730-737.

1039 Stow, D.A.V., and Piper, D.J.W., 1984. Deep-water fine-grained sediments: facies models. In Stow,
1040 D.A.V., and Piper, D.J.W. (Eds.). Fine-grained sediments: deep-water processes and facies.
1041 Special Publications, Geological Society of London, 14, pp. 611-645.

1042 Stow, D.A.V., Howell, D.G., and Nelson, C.H., 1985. Sedimentary, tectonic, and sea-level controls, in
1043 Bouma, A.H., et al., eds., Submarine fans and related turbidite systems. New York, Springer,
1044 p. 15–22.

1045 Stow, D.A.V., Howell, D.G., Nelson, C.H., 1984. Sedimentary, Tectonic, and Sea-Level Controls on
1046 Submarine Fan and Slope-Apron Turbidite Systems. Geo-Marine Letters 3, 57-64.

1047 Stow, D.A.V., Shanmugam, G., 1980. Sequence of structures in fine-grained turbidites: comparison of
1048 recent deep-sea and ancient flysch sediments. Sedimentary Geology 25, 23–42.

1049 Sumner, E.J., Siti, M.I., McNeill, L.C., Talling, P.J., Henstock, T.J., Wynn, R.B., Djajadihardja, Y.S.,
1050 Permana, H., 2013. Can turbidites be used to reconstruct a paleoearthquake record for the
1051 central Sumatran margin? Geology, doi:10.1130/G34298.1

1052 Swan, A.R.H., Sandilands, M., 1995. Introduction to Geological Data Analysis. Blackwell Science,
1053 Oxford; Cambridge, Mass, USA.

1054 Sylvester, A.G., 1988. Strike-slip faults. Geological Society of America Bulletin 100, 1666-1703.

1055 Tabachnick, B.G. and Fidell, L.S., 2007. Using Multvariate Statistics, Fifth Edition, Boston: Pearson
1056 Education, Inc.

1057 Talling, P.J., 2014. On the triggers, resulting flow types and frequencies of subaqueous sediment
1058 density flows in different settings. Marine Geology 352, 155-182

1059 Talling, P., Clare, M., Urlaub, M., Pope, E., Hunt, J., & Watt, S. (2014). Large Submarine Landslides
1060 on Continental Slopes: Geohazards, Methane Release, and Climate Change. Oceanography,
1061 27 (2), 32-45.

1062 Talling, P.J., Masson, D.G., Sumner, E.J., Malgesini, G., 2012. Subaqueous sediment density flows:
1063 depositional processes and deposit types. Sedimentology 59, 1937-2003.

1064 Talling, P.J., Paull, C.K., Piper, D.J.W. 2013. How are subaqueous sediment density flows triggered,
1065 what is their internal structure and how does it evolve? Direct observations from monitoring
1066 of active flows. Earth-Science Reviews 125. 244-287.

1067 Thomson, J., and Weaver, P.P.E., 1994. An AMS Radiocarbon method to determine the emplacement
1068 time of recent deep-sea turbidites. Sedimentary Geology 89, 1–7.

1069 Tsutsui, B., Campbell, J.F., Coulbourn, W.T., 1987. Storm-generated, episodic sediment movements
1070 off Kahe Point, Oahu, Hawaii. Marine Geology 76, 281–299.

1071 Urlaub, M., Talling, P., & Clare, M. (2014). Sea-level-induced seismicity and submarine landslide
1072 occurrence: Comment. Geology 42 (6), 337.

1073 Urlaub, M., Talling, P. J., & Masson, D. G. (2013). Timing and frequency of large submarine
1074 landslides: implications for understanding triggers and future geohazard. Quaternary Science
1075 Reviews 72, 63-82.

1076 Vail, P.R., Mitchum, R.M.J., Todd, R.G., Widmier, J.M., Thompson, S.I., Sangree, J.B., Bubb, J.N.,
1077 Hatelid, W.G., 1977. Seismic stratigraphy and global changes of sea level. In: Payton, C.E.
1078 (Ed.), Seismic Stratigraphy – Applications to Hydrocarbon Exploration. AAPG Mem., vol.
1079 26. American Association of Petroleum Geologists, Tulsa, Ok, pp. 49–212.

1080 van Rooij, M.M., Nash, B.A., Rajaraman, S., Holden, J.G., 2013. A fractal approach to dynamic
1081 inference and distribution analysis. Frontiers in Physiology 4.

1082 van Weering, T.C.E., de Stigter, H.C., Boer, W., de Haas, H., 2002. Recent sediment transport and
1083 accumulation on the NW Iberian margin. Progress in Oceanography 52, 349-371

1084 Vanney, J-R., Mougenot, D., 1990. Un canyon sous-marin du type ’gouf’: le Canhao da Nazare´
1085 (Portugal). Oceanologica Acta 13, 1–14

1086 Villamor, P., Capote, R., Stirling, M.W., Tsige, T., Berryman, K.R., Martinez-Diaz, J.J., Martin-
1087 González, F., 2012. Contribution of active faults in the intraplate area of Iberia to seismic
1088 hazard: The Alentejo-Plasencia Fault. Journal of Iberian Geology 38 (1), 85-111.

1089 Vittinghoff, E., and C. E. McCulloch (2007), Relaxing the rule of ten events per variable in logistic
1090 and Cox regression, American Journal of Epidemiology, 165(6), 710.

1091 Weaver, P. P. E., 1994. Determination of turbidity current erosional characteristics from reworked
1092 coccolith assemblages, Canary Basin, north-east Atlantic. Sedimentology 41, 1025–1038.
1093 Weaver, P.P.E., Thomson, J., 1993. Calculating erosion by deep-sea turbidity currents during
1094 initiation and flow. Nature 364, 136–138.
1095 Wynn, R.B., Weaver, P.P.E., Stow, D.A.V., Masson, D.G., 2002. Turbidite depositional architecture
1096 across three interconnected deep-water basins on the northwest African margin.
1097 Sedimentology 49, 1441–1462.
1098 Xu, J.P., Noble, M.A., Rosenfeld, L.K., 2004. In-situ measurements of velocity structure within
1099 turbidity currents. Geophysical Research Letters 31, L09311, doi:10.1029/2004GL019718.

1100 Zitellini, N., Rovere, M., Terrinha, P., Chierici, F., Matias, L., and Bigsets Team, 2004. Neogene
1101 Through Quaternary Tectonic Reactivation of SW Iberian Passive Margin. Pure and Applied
1102 Geophysics 161, 565–587.

1103

1104 Figures and Tables:

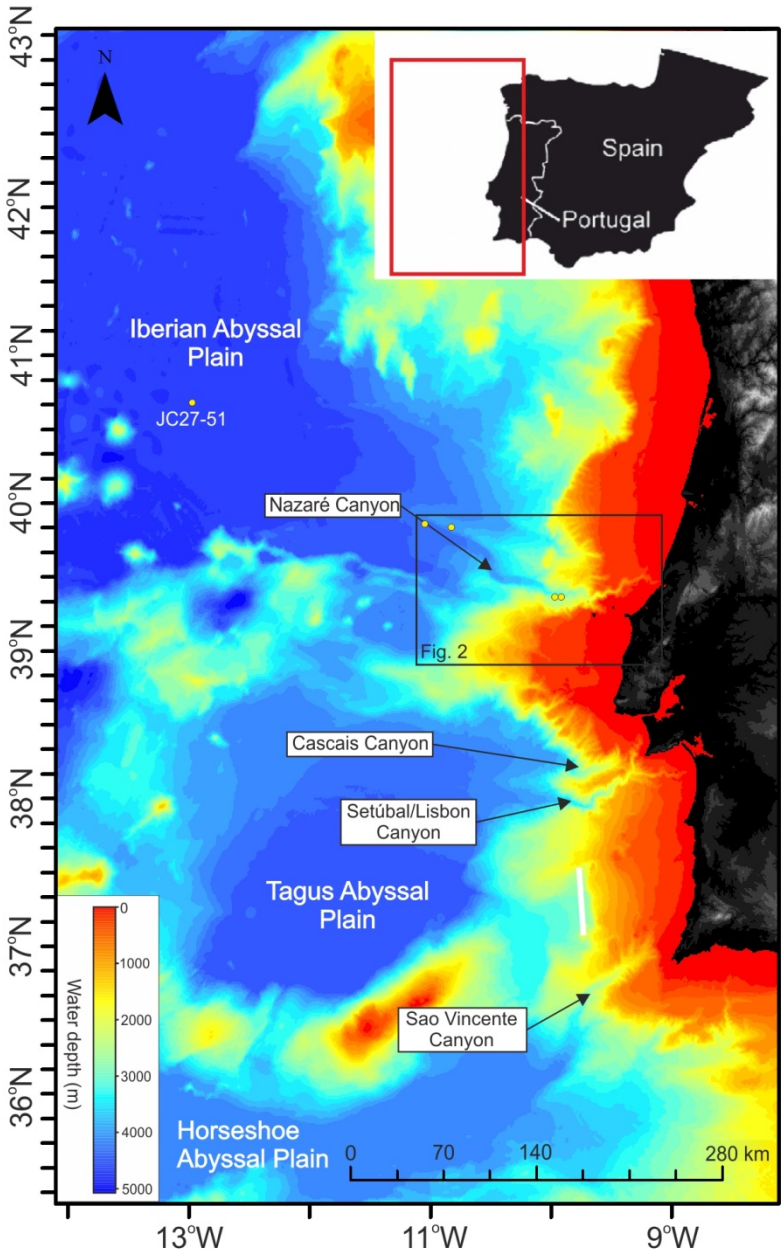

1105

1106 Fig. 1: Map of the Portuguese Margin, showing the location of the main sedimentary basins and their
1107 feeder canyons. Core JC27-51, located in the distal Iberian Abyssal Plain is also shown. Bathymetry
1108 data are from the GEBCO database (IOC, IHO, BODC, 2003).

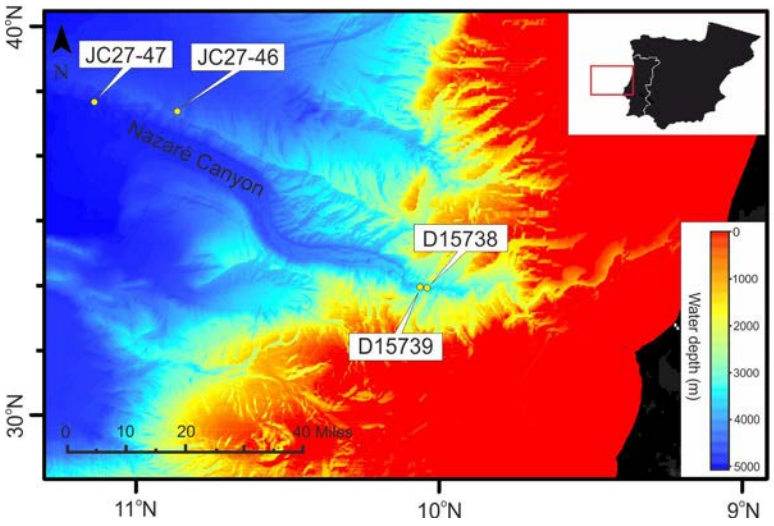

Fig. 2: Location map of the Nazaré Canyon and the locations of canyon cores used in this study.

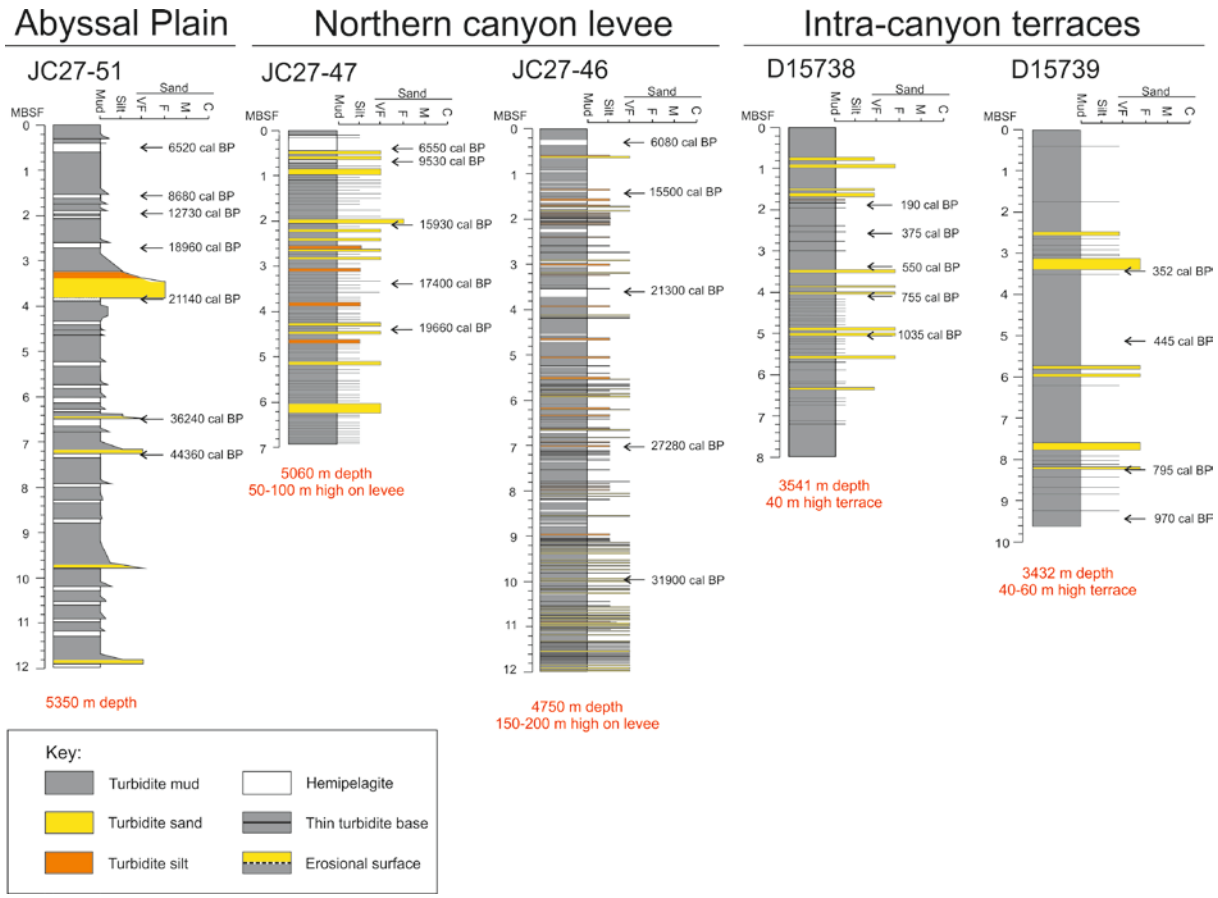

Fig. 3: Lithological description of the cores used in this study. Dark grey represents turbidite mud, orange represent silt and yellow represents sand. Radiocarbon dates and their core positions are indicated with black arrows.

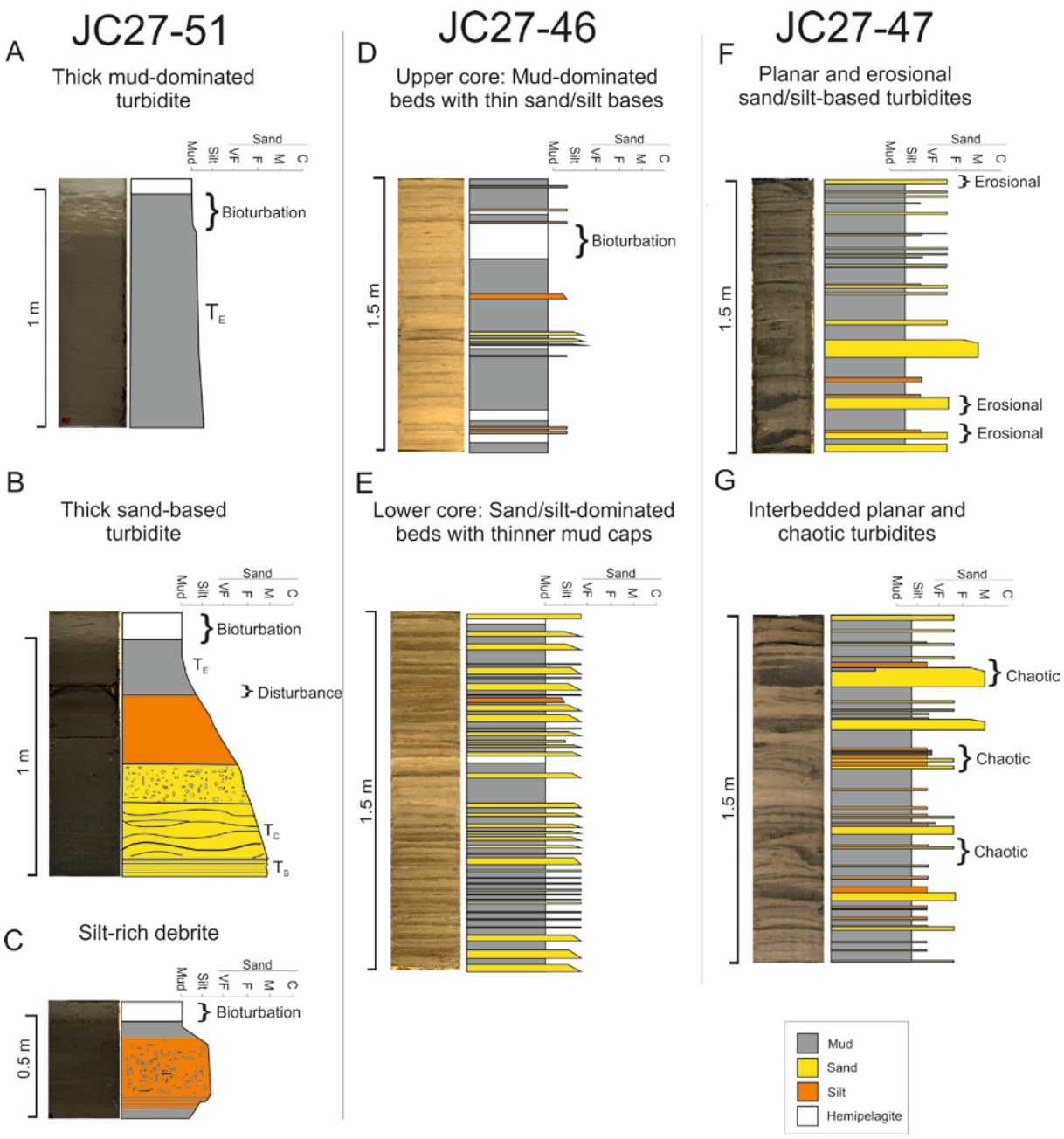

Fig. 4: Bed types present in JC27 sediment cores. JC27-51: (A) Thick mud-dominated turbidites wich bioturbated mud caps, (B) thick sand rich turbidites with discernible Bouma (T) divisions , and (C) a debrite with mud and silt clasts. JC27-46: (D) The upper 6 m of the core is composed of thin sand or silt-based turbidite with a dominant mud unit and hemipelagic sediment intervals. (E) The lower 6m is mainly composed of thin-bedded sand rich turbidites with a thinner mud cap and sparse hemipelgic sediment. JC27-47: Turbidites are typically (F) planar and often erosive, or (G) chaotically structured, with reverse grading, overturned layers and evidence of scouring.

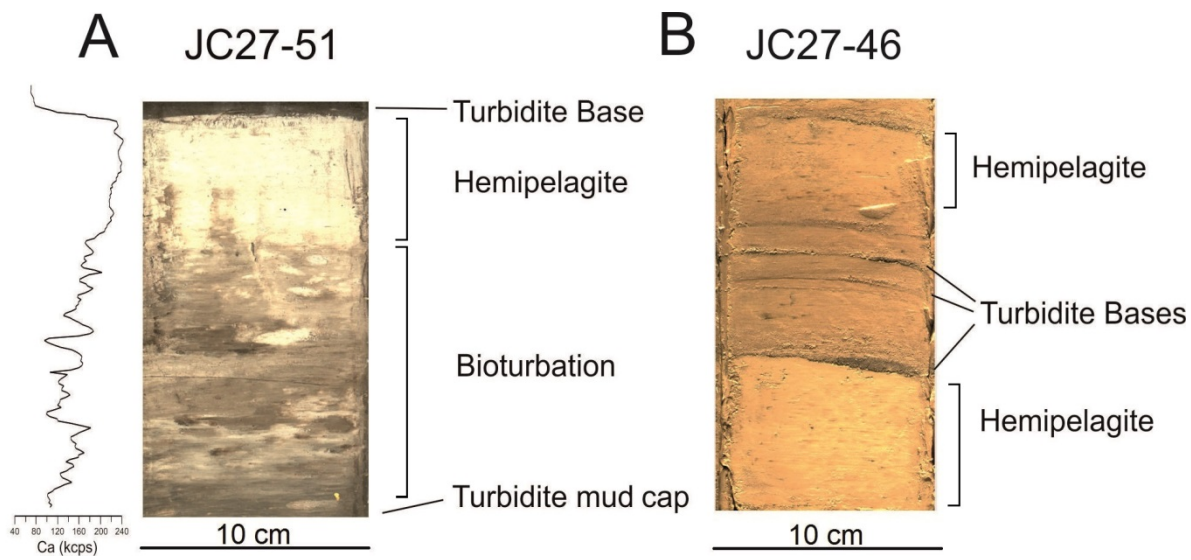

Fig. 5: Hemipelagic material and turbidites present within cores JC27-51 and JC27-46. ITRAX Calcium records assist in defining the boundaries between pure hemipelagite and bioturbated turbidite mud cap in JC27-51. There are no ITRAX data for JC27-46, but hemipelagite can still be defined by the presence of a colour change and dark mottling.

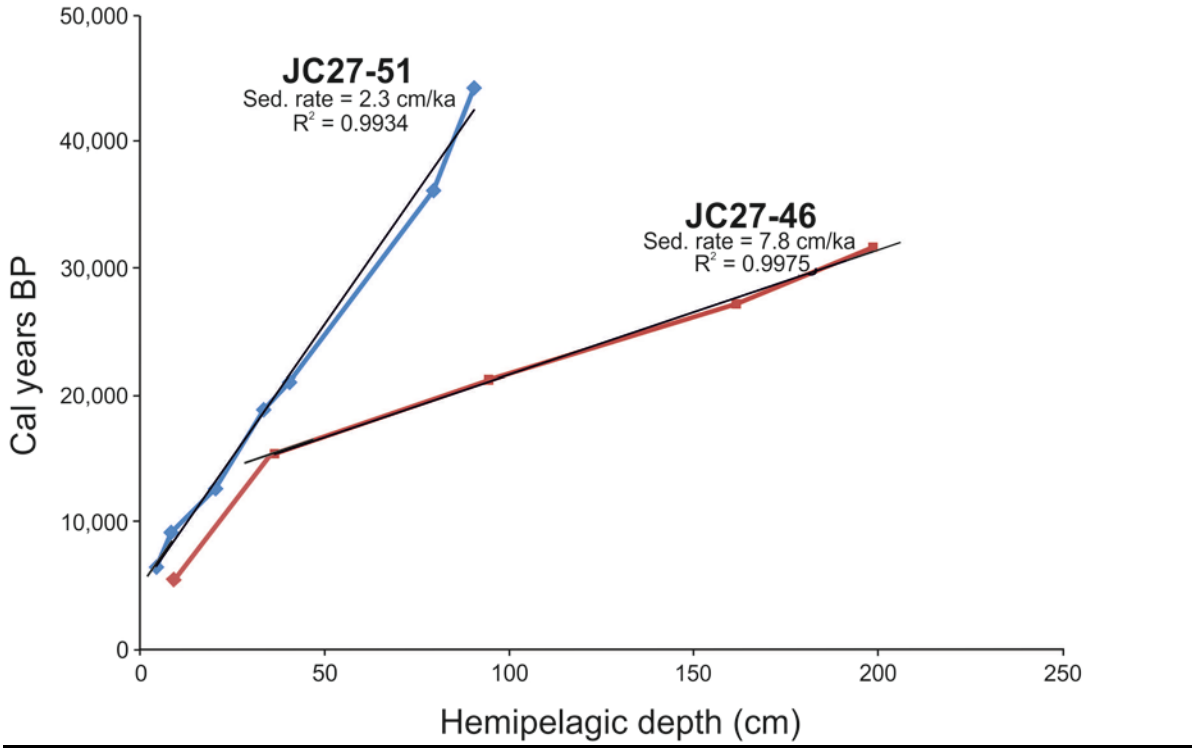

Fig. 6: hemipelagic aGe models for cores JC27-51 and JC27-46. R^2 values indicate minimal deviation from the line and thus a relatively stable hemipelagic sedimentation rate in both cores. This serves as a reasonable basis for using a stable sedimentation rate to interpolate between radiocarbon dates and further back in the record beyond radiocarbon age.

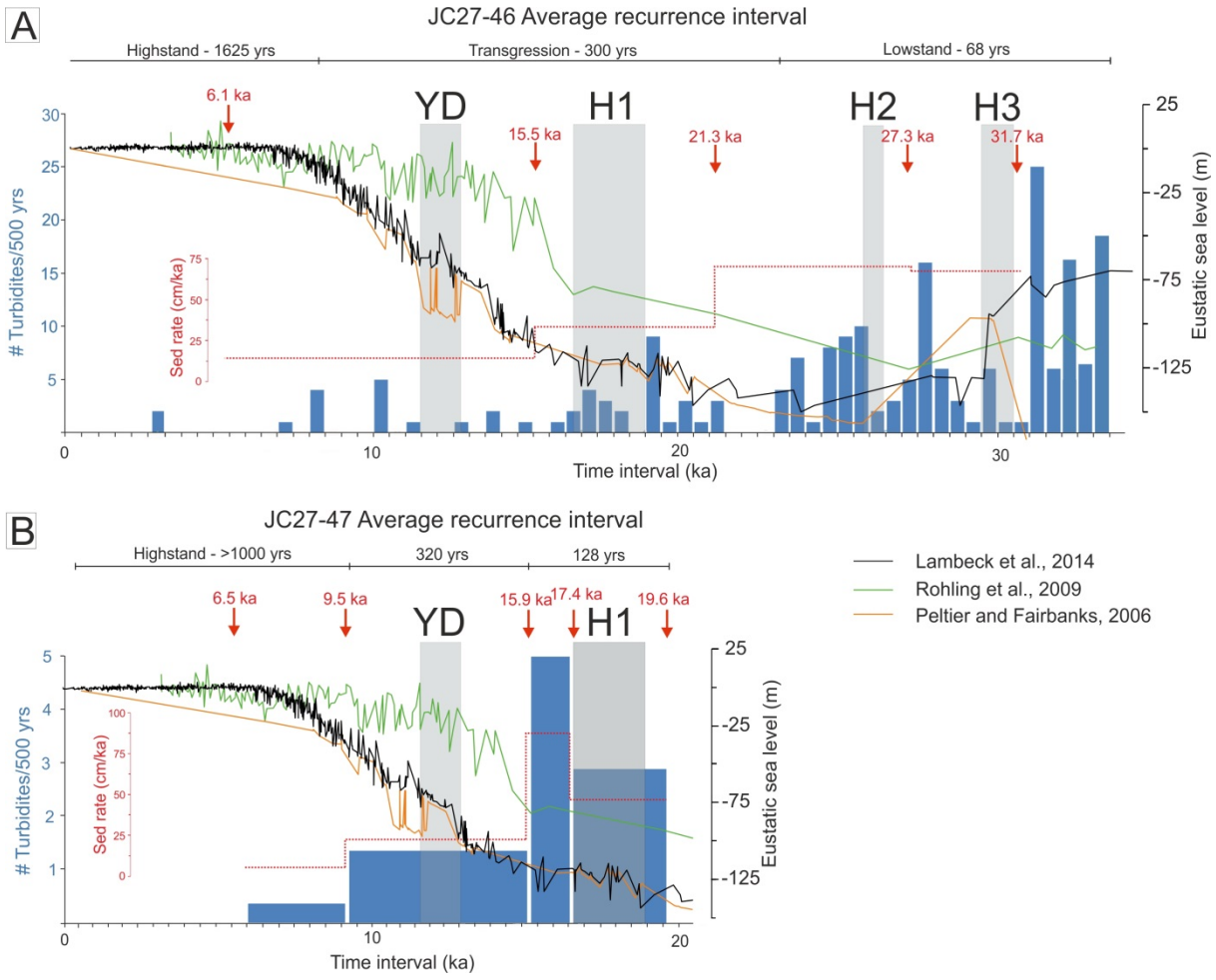

1133

1134 Fig. 7. **A**: Frequency of turbidites contained within core external levee JC27-46. Turbidites are binned
1135 into 500 year intervals and plotted against global eustatic sea level curves. Trend suggests near
1136 shutdown of large canyon-filling turbidites recorded in the levee following the onset of sea level
1137 highstand at 7 ka. **B**: Frequency of turbidites from internal levee core JC27-47. It illustrates a similar
1138 pattern of decline through sea level transgression and into the present-day highstand. H1-3 = Heinrich
1139 events. YD = Younger Dryas.

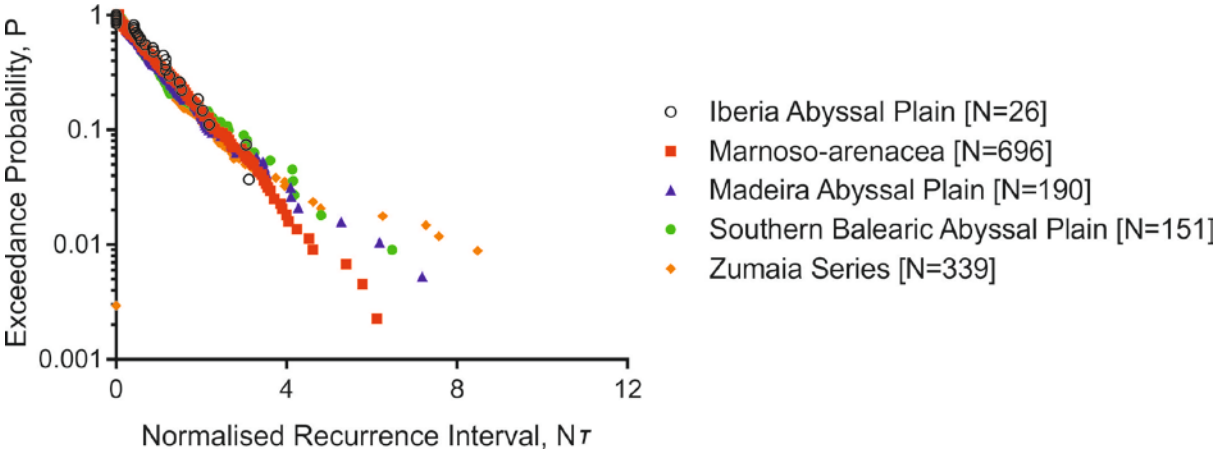

1140

Fig. 8: Comparison of Iberian Abyssal Plain recurrence intervals with published recurrence intervals from several long-term basin records in Clare et al. (2014). The vertical axis plots the probability (P) that a given turbidite recurrence interval value (time since last event, T) will exceed the average recurrence interval for its respective dataset. The horizontal axis plots normalised recurrence interval data. The recurrence intervals are normalized by subdividing each recurrence interval (T) by the mean recurrence interval (λ) for each of the data sets to plot a dimensionless variable, R_T. N = number of events in each basin data series.

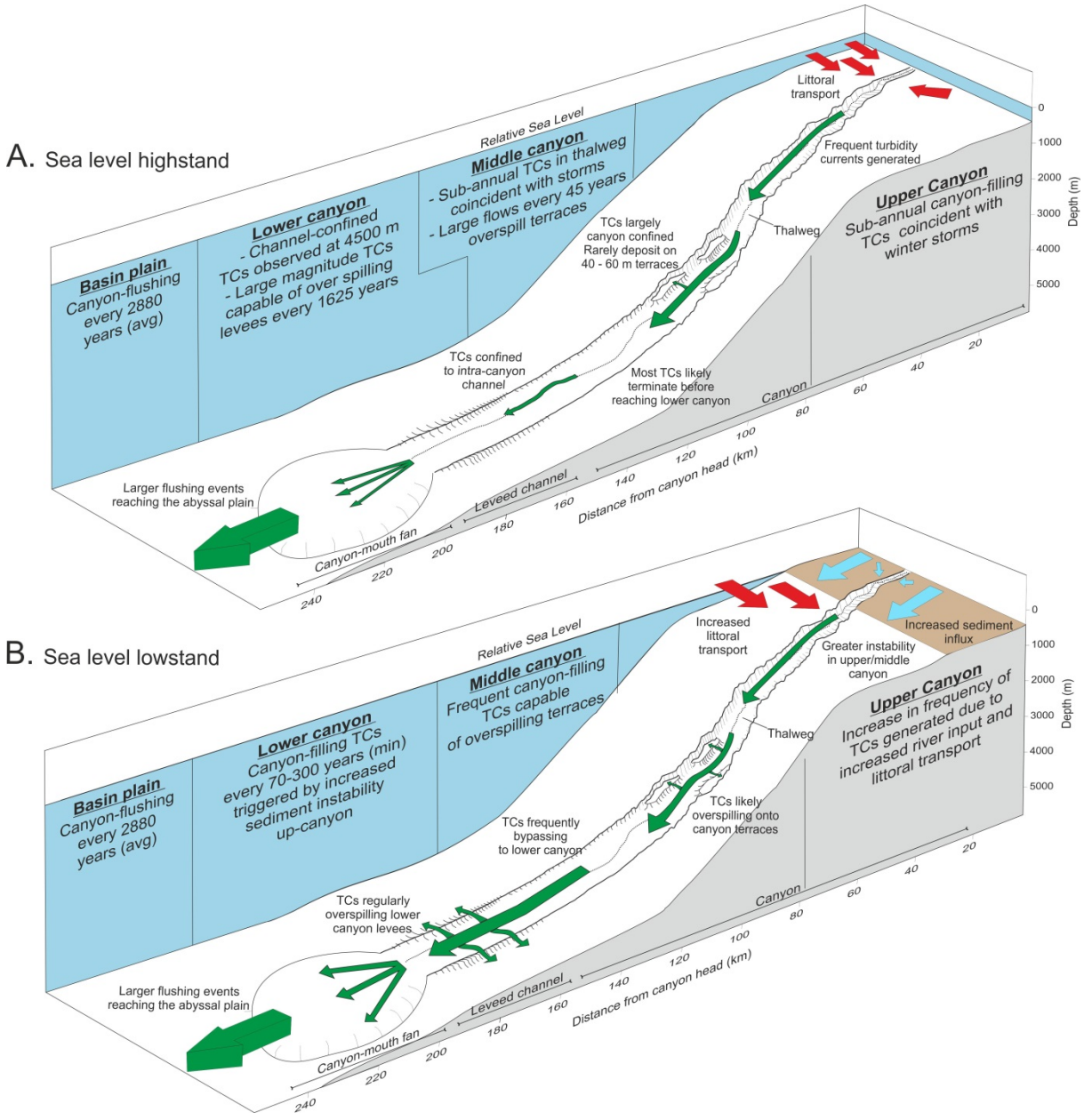

Fig. 9: Schematic displaying the spatial and temporal variability in turbidity current frequency in Nazaré Canyon during periods of sea level lowstand and highstand. **A**: During the present day

highstand canyon-filling turbidity currents (TCs) are frequent in the upper canyon, but only small thalweg-confined turbidity currents reach to greater than 4,000 m water depth. **B**: During lowstand conditions canyon-filling turbidity currents were much larger, were able to reach the lower canyon, and regularly over-spilled canyon levees. Infrequent canyon-flushing turbidity currents were not affected by changes in sea level and continued into the present-day highstand.

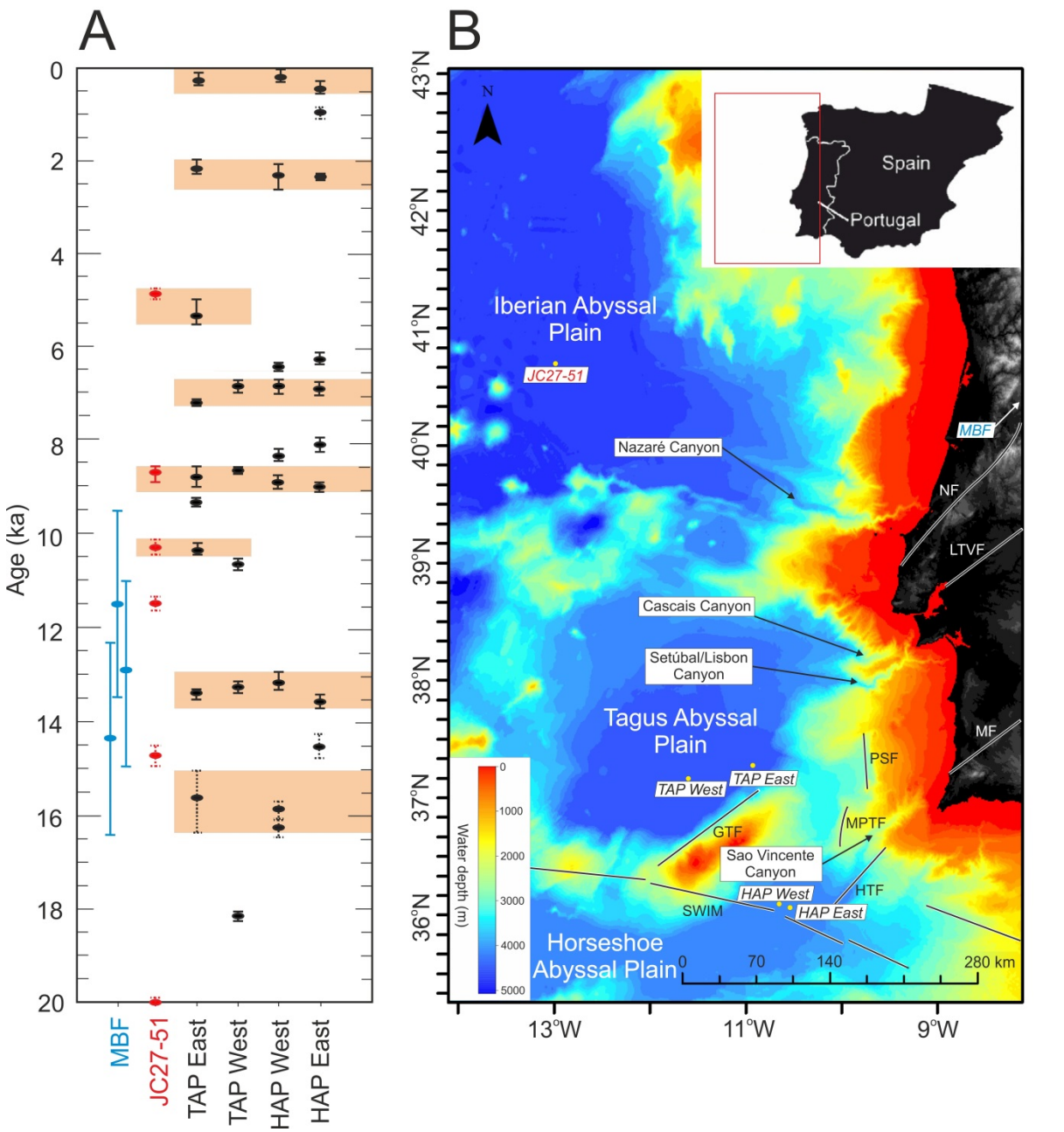

Fig. 10. **A**: Proposed seismoturbidites from the Tagus and Horseshoe Abyssal Plains from Grácia et al. (2010) and Masson et al. (2011b) (shown as black dots). Turbidites from the Iberian Abyssal Plain are shown in red, and paleoearthquakes from the Manteigas-Braçanga Fault are shown in blue. Orange

bars represent event which can be correlated based on their age uncertainties. Dashed error bars on ages represent ages that are determined through linear interpolation. **B**: Map of the Portuguese Margin showing primary structural faults. MTB = Manteigas-Braçanga Fault, NF = Nazaré Fault, LTVF = Lower Tagus Valley Fault, MF = Messejana Fault, PSF = Pereira de Sousa Fault, MPTF - Marquês de Pombal Thrust Fault, HTF = Horseshoe Thrust Fault, GTF = Gorringe Thrust Fault, SWIM = South-western Iberian Margin lineaments. Labels in italics indicate locations of paleoseismic reconstructions in Fig. 10A.

Lab code	Core #	Core depth (cm)	Conventional age (BP)	Max. probabilty (Cal BP)	1σ Cal age ranges (Cal BP)	2σ Cal age ranges (Cal BP)	Source
BETA-385402	JC27-46	32-33	5,940 ± 30	6,078	5,995-6,165	5,918-6,233	This study
BETA_385403	JC27-46	158-159	13,639 ± 50	15,494	15,334-15,629	15,234-15,768	This study
BETA_385404	JC27-46	349-350	18,290 ± 60	21,303	21,143-21,465	20,994-21,599	This study
BETA_385405	JC27-46	701-702	23,600 ± 100	27,280	27,163-27,406	27,020-27,514	This study
BETA_385406	JC27-46	996-997	28,790 ± 140	31,750	31,568-32,146	31,449-32,521	This study
SUERC-31798	JC27-47	53-54	6,120 ± 35	6,270	6,197-6,341	6,117-6,422	This study
BETA-401321	JC27-47	70.5-71.5	8,510 ± 30	8,760	8,652-8,889	8,584-8,972	This study
SUERC-31799	JC27-47	212-214	13,530 ± 47	15,300	15,201-15,479	15,117-15,638	This study
BETA-401322	JC27-47	340-341.5	14,910 ± 50	14,700	17,211-17,469	17,089-17,576	This study
SUERC-31802	JC27-47	445-448	16,910 ± 55	19,580	19,484-19,725	19,360-19,894	This study
	JC27-51	48.5-49.5	6,355 ± 37	6,520	6,433-6,604	6,342-6,680	This study
BETA-382057	JC27-51	155-156	8,470 ± 30	8,680	8,604-8,769	8,567-8,893	This study
	JC27-51	196.5-197.5	11,535 ± 39	12,730	12,661-12,810	12,613-12,904	This study
	JC27-51	264-265	16,415 ± 53	18,960	18,883-19,083	18,808-19,206	This study
	JC27-51	381-382	18,196 ± 62	21,140	21,019-21,322	20,886-21,469	This study
BETA-382053	JC27-51	649-650	33,010 ± 200	36,240	36,000-36,454	35,722-36,719	This study
BETA-382054	JC27-51	726-727	41,500 ± 550	44,360	43,825-44,875	43,310-45,314	This study
SUERC-18143	D15738	178.5	573 ± 37	190		90-290	Masson et al, 2011a
SUERC_18146	D15738	250.5	738 ± 37	375		290-460	Masson et al, 2011a
SUERC_18147	D15738	335	934 ± 37	550		480-620	Masson et al, 2011a
SUERC_18148	D15738	405	1,204 ± 37	755		660-850	Masson et al, 2011a
SUERC_18149	D15738	509.5	1,482 ± 35	1,035		940-1,130	Masson et al, 2011a
SUERC-18150	D15739	334.5	703 ± 37	352		270-435	Masson et al, 2011a
SUERC-18151	D15739	489.5	821 ± 37	445		370-520	Masson et al, 2011a
SUERC-18153	D15739	829.5	1,245 ± 37	795		700-890	Masson et al, 2011a
SUERC-18156	D15739	959.5	1,411 ± 37	970		890-1,050	Masson et al, 2011a

Table 1: List of radiocarbon samples used in this study. Note: Cal BP ages from D15738 and D15739 (Masson et al, 2011a) are median values, and not determined using maximum probability.

Turbidite no	Turbidite base depth (cm)	Turbidite thickness (cm)	Approx age (cal BP)	Recurrence interval (years)
1	25	25	4,850	0
2	45	20	4,850	4,430
3	155	103	8,680	1,700
4	172	13	10,300	0
5	187	15	10,300	1,200
6	194	4	11,505	3,200
7	254	53	14,700	5,550
8	378	110	20,250	1,350
9	428	46	21,600	1,500
10	454	22	23,100	0
11	468	14	23,100	0
12	503	35	23,100	1,600
13	523	16	24,700	2,550
14	570	40.5	27,250	1,950
15	597	24	29,200	4,300
16	618	10	33,500	1,200
17	645	24	34,700	9,000
18	671	12.5	43,700	0
19	725	54	43,700	3,600
20	790.5	57.5	47,300	5,850
21	837	36	53,150	1,250
22	870	30.5	54,400	8,800
23	978	102	63,200	3,350
24	1016	38	66,550	3,350
25	1050	26	69,900	6,300
26	1091	36	76,200	2,500
27	1119	20	78,700	3,350
28	1187	60	82,050	
				Avg: 2800

Table 2: Core JC27-51 turbidites, their projected ages, and recurrence interval determined using a linear age model.